Reply to Referee 1. We indicate a referee comment with "Referee" and our response with "Authors".

Referee: I have a multitude of concerns with this work, and believe that the paper should not be published in its current form. My primary one is that the "new" CLARRA algorithm is almost exactly the same as the so-called "MIXCRA" algorithm of Turner (J Appl Meteor, 2005). In fact, it is almost like the authors were trying to disguise this as there is not a single reference to the MIXCRA paper in sections 1, 2, 3.1, or 3.2; yet it is clear the authors know about MIXCRA because it is referenced at the top of section 3.3. It is not clear what makes CLARRA different from MIXCRA.

Authors: Our main purpose is to inform instrument development by quantifying the effect of instrument resolution on cloud property retrievals, which to our knowledge is novel and within the scope of AMT. Furthermore, aspects of CLARRA are novel, including formulations for matching instrument resolution for the cloud property retrievals, as described in Section 3.1. Other novel aspects of this work include testing retrievals on a wide set of simulations that are meant to be characteristic of the annual cycle of Arctic clouds and atmosphere (based on previous work by the authors; including different ice habits and vertically-varying clouds; Section 2) and quantifying the effect on the retrieval of a range of errors in the instrument and atmospheric state (Section 4). We have modified the paper throughout to make the purpose clearer.

Given our main purpose, we do not see similarities between CLARRA and published work as a source of concern. The optimal nonlinear inverse method in CLARRA is similar to MIXCRA (Turner 2005) and to other work, as cited in the submitted manuscript: "The inverse method is similar to the method of Turner (2005) which has been used to retrieve cloud properties from AERI instruments in the Arctic (Turner 2005; Cox et al 2014). Similar inverse methods have also been used from satellite instruments (L'Ecuyer et al 2006; Wang et al 2006)." To make this clearer, we have combined these sentences and added references to Poulsen et al., 2012 (and L'Ecuyer et al, 2019, in response to reviewer 2). Also, it should be noted that polar cloud property retrievals in general build on a large body of published work, including work by the authors (Mahesh et al 2001; Rathke et al 2002a,b).

We do not see the relevance of the MIXCRA paper to Section 2, which is based on Cox et al, 2016, or to Sections 3.1 or 3.2, which we believe are largely novel to our work (note that the revised manuscript is restructured somewhat following Reveiewer 2). However, we realize that our results and discussion section would benefit from comparison to published work by Turner 2005 and others. Therefore we will add text such as the following to Section 5.1:

"We find that the retrievals lose sensitivity to COD between about 4 and 10 (see Sect. 5.2 below); in previous work retrieving cloud properties from downwelling IR radiances in a similar wavenumber range, cut-offs of 4 to 6 were used (Mahesh et al 2001; Rathke 2002a,b; Turner 2005). Here, we constrain the retrievals to an optical depth of 10 and focus primarily on results for optical depths <= 4. The retrievals were found to lose sensitivity to effective radius above about 50 μm (see Supplemental), which is in keeping with Rathke and Fischer (2000) and Garrett and Zhao (2013), but differs from the cut-off values of 25 μm used by Mahesh et al (2001) and of 100 μm by Turner (2005)."

Because CLARRA has similarities to a variety of algorithms, it is beyond the scope of this work to detail them all. However, we provide sufficient detail to determine differences by comparing our paper to the published literature. For example, differences in CLARRA relative to MIXCRA include:

1) **CLARRA includes a cloud height retrieval (Section 3; the revised manuscript also mentions this in the introduction).**
2) **CLARRA includes a forward retrieval that is computationally fast (Section 3.2).**
3) **CLARRA accounts for gaseous emission at instrument resolution using a novel method (convolving radiances and transmittances with the instrument lineshape; Section 3.1 in the submitted manuscript).**
4) **The optimal nonlinear inverse method in CLARRA uses the Levenberg-Marquardt formulation, and uses the radiance as the observation (the variable y in Rodgers 2000; *R* in Eqn (16) in the submitted manuscript).**
5) **CLARRA uses temperature-dependent liquid water refractive indices (Section 3.2).**
6) **CLARRA is written primarily in Python and calls DISORT directly from Python via f2py.**

Referee: My second primary concern is simply: Is this paper really adding any new knowledge? I presume that they are using observations in spectral regions that are between absorption lines (these are often called "microwindows"), and the cloud properties in these microwindows are essentially unchanged. This allows the radiance to be averaged from higher spectral resolution to that of the width of the microwindow; this was done in the MIXCRA paper (see Table 1 in that paper). Indeed, the microwindows used in the MIXCRA paper are between 2 and 8 cm-1 wide, depending on the spectral region. So while the MIXCRA paper didn't specifically test retrievals performed at 0.5 vs. 4 cm-1, it already is showing the impact.

Authors: We understand the point that averaging over microwindows implies that resolution is not very important, but the issue is more complex because strong gaseous emission lines bleed into the microwindows at coarser resolution, so that there is still a need to quantify the effect of resolution. The reason microwindows are used is to minimize the contribution of emission by gases. Gaseous emission lowers sensitivity to cloud and enhances errors. At a resolution of 0.1 cm^{-1}, in a microwindow of 4 cm^{-1}, the contribution from gaseous absorption lines outside the microwindow will be minimal. However, as resolution gets coarser, the gaseous absorption lines bordering the microwindow contribute more and more, decreasing sensitivity and increasing errors. To design a lower-resolution instrument, it is essential to quantify these errors to determine at what resolution they become important. We have added text similar to that above to Section 3.1.

Furthermore, resolution affects the accuracy of cloud height retrievals, which in turn affects the accuracy of microphysical cloud property retrievals, as discussed in the manuscript. Thus, our paper adds new knowledge by quantifying how cloud-property retrievals depend on resolution, from 0.1 to 8 cm^{-1}. To make this more clear, we increased the resolution range to 20 cm^{-1} and included more discussion of how cloud-height retrieval accuracy affects the accuracy of microphysical cloud property retrievals.

Referee: [As a side note: the authors really do need to include a table on what microwindows are being used in this study.

Authors: A table showing the microwindows was included in the Supplemental and discussed in Section 3: "Selected microwindows (see Supplemental) are similar to those in Turner

(2005) …" We have moved the table into the main text, added a second set of microwindows (see the response to the final comment), and added the relevant references.

Referee: In addition to the actual microwindows, if the microwindow is actually only 4 cm-1 wide, do the authors limit their spectral width of that "channel" to only or do they include the absorption lines that exist on the sides of these microwindows? If they are testing 0.1 cm-1 resolution, do they allow multiple "channels" within a given microwindow, or only a single channel? Without this information, the results here cannot be reproduced.]

Authors: Section 3.1 described calculation of radiances and transmittances (Eqns 1-8) and states that they are then averaged within microwindows; these are then used to compute effective-resolution optical depths (Eqns 9-10). For the observations (which here are simulations), radiances are averaged in the microwindows. Using the equations and microwindows provided, our results should be reproducible. (Note that much of Sect. 3.1 was moved to the Appendix, following the suggestions of Reviewer 2; we also made changes for clarity).

Referee: The uncertainties assumed for temperature and humidity profiles in the reanalysis (around line 355) are shockingly small. These uncertainties might be true for a large average, but in a scene-by-scene way the errors will be much, much larger. For example, if the reanalysis believes that the sky is cloud-free above the instrument, there analysis may have developed a surface-based inversion that would not be there in reality because of the cloud. An example of how the presence of a cloud modifies the temperature profile beneath the cloud is given by Miller et al. JGR 2013 (which includes Walden as a coauthor). Because clouds are so hard to represent properly in large-scale models, I think the authors need to use more representative uncertainties (e.g., many degrees for temperature, and at least 20% for water vapor) for the temperature and humidity profiles, and show the impact of these uncertainties.

Authors: We believe use of the mean error is reasonable. According to Wesslen et al (2014) the 95% confidence interval is within 0.3 K for temperature and within a few percent for humidity. Also, as noted in the text, bias errors in humidity or temperature give similar results as considerably larger errors that vary in sign with height, which is likely for reanalysis data (Wesslen et al, 2014). Finally, note that in addition to the mean errors, we tested the effect on the retrieval of errors in water vapor as high as a 10% bias at all heights. We have added retrievals for a temperature bias of 1 K, increased error magnitudes in combinations of errors, and changed "typical errors expected" to "biases" in the abstract. (Our main conclusions are unaffected).

Referee: The authors are using the far-infrared for several of their channels; indeed, using those channels are really important for discriminating the cloud phase (see Turner et al. JAM2003 as well as Turner JAM 2005).

Authors: Yes. This point was published prior to these papers by Rathke et al (2002), whom we reference:

Rathke, C., Fischer, J., Neshyba, S., & Shupe, M. (2002). Improving IR cloud phase determination with 20 microns spectral observations. Geophysical Research Letters, 29(8), 50–1–50–4. http://doi.org/10.1029/2001GL014594.

Referee: However, water vapor absorbs strongly in the far-infrared, and if the PWV is large enough the window will be opaque purely due to water vapor absorption. Thus, the range of cloud optical depth that can be sensed depends strongly on the PWV; this needs to be discussed in this paper.

Authors: This is a good point. We have changed Section 2 to clarify that the range of PWV varied from 0.2 to 3 cm, which previous work has shown is appropriate for polar regions. For this range of PWV, the far IR window was not opaque.

Referee: I think that the authors have missed a real opportunity to talk about how the uncertainties in the retrieved products covaries (i.e., by looking at the off-diagonal elements of the posterior covariance matrix). This was one of the shortcomings of the MIXCRA paper, and expansion of that here would add some new insights to the community. For example, as the cloud emissivity moves towards unity, there will likely be a high amount of correlated error between Reff,ice and Reff,liq. Ditto when the cloud emissivity is small. How does the ice fraction uncertainty covary with the other retrieved variables, especially in different areas of the solution space? A different question along the same lines as above is this: does the accuracy and covariance between the cloud properties change if the retrieval is configured to retrieve (total_tau, ice_fraction, Reff_ice, Reff_liq) vs. (tau_liq, tau_ice, Reff_ice, Reff_liq)? The MIXCRA algorithm was initially the first (in JAM 2005), but was changed to the latter (Turner and Eloranta TGRS 2008) and showed pretty good results relative to the HRSL during MPACE.

Authors: We agree that this would be interesting. However, it is beyond the scope of the current paper. We will look into this in future work.

Referee: The authors really didn't spend any time discussing the different technologies that could be used to provide these radiance observations, or why they would be "cheaper" from the instrument that they assumed (which seems to be the AERI). Radiometers using a finite number of channels with bolometers as detectors are one possibility; there are many papers by the so-called "TICFIRE" project being run out of the Canadian Space Agency that might be useful. But how important is the calibration of cheaper systems like this?

Authors: We have added a few comments indicating additional design factors that could be useful (Section 5.2). More in-depth discussion of instrument development is beyond the scope of this work but is an important subject for future work.

Referee: The authors did show results if the radiance bias was 0.2 RU, but that is a pretty small error – a more realistic error might be 1 or 2 RU. Do these results scale? [For example, even with a carefully calibrated AERI, radiance biases close to 1 RU have been reported – see Delamere et al. JGR 2010. It is hard to imagine that a cheaper radiometer would have better spectral calibration than the AERI.]

Authors: We have added retrievals for radiance biases of 0.5 RU (Supplemental) and 1 RU (main text).

Referee: Some more minor points:

How many streams are being used in DISORT? Fewer streams make the RT code faster, but will decrease the accuracy.

Authors: This is a good point. We generally use 16 streams, but we had previously used fewer for smaller particles (when only a few Legendre moments are needed for the phase function), but after communicating with the DISORT group, we re-ran all cases with 16 streams. This had a small effect on retrievals, and model errors are lower. We have added text to the end of Section 3.3 indicating that DISORT is run with 16 streams.

Referee: Eq 18 is incorrect if gamma > 0. The correct formulation was originally provided by Masiello et al. QJRMS2012, but was also presented in Turner and Löhnert JAMC 2014.

Authors: We use Eq. 18 because iterations are repeated until gamma is negligibly small (<0.01). This is clarified.

Referee: "the ideal range for tau is between 0.4 and 5" (line 425). The authors really should indicate how often this is expected to happen in the Arctic. The Cox et al. JAMC 2014 paper provides some information on this, at least for that site.

Authors: This is a good point. We will add text such as the following to address this:

To get a sense of how common such clouds are, Cox et al 2014 found that at Eureka, Nunavut in 2006-2009, clouds with optical depths of 0.25 to 6 accounted for about 32% of AERI measurements (17% when quality control procedures and a PWV threshold of 1 cm were applied; in this work PWV is as high as 3 cm).

Referee: Is there a minimum number of spectral microwindows that need to be used? Stated a different way, how do the errors in the retrieved cloud properties change for different microwindow subsets?

Authors: This is an interesting topic. We have tested a second set of wavenumbers and reported differences. We agree that further sensitivity studies along these lines would be interesting; however they are beyond the scope of this work.

Reply to Referee 2. We indicate a referee comment with "Referee" and our response with "Authors".

Referee: The methodology is clearly stated, adequate references are made to work by earlier studies although more recent articles may be available, and the analyses are straight-forward. I am glad to see that the software is being made available to the community as described in Section 7. My view is that the paper is suitable for publication pending relatively minor revisions that address the comments that follow.

If there is one primary suggestion to offer, it would be to compare the cloud prop-erties obtained by this method to those obtained from CALIPSO, where new Version4 products are now available (or to a coincident ground-based lidar if possible). Of particular note is that the V4 products have significant improvements in calibration and cloud/aerosol properties. There will be differences between satellite- and surface-based products that will bear further investigation, but this may be outside the scope of this particular study. CALIPSO cloud products have been used heavily in the development and testing phase of many satellite-based cloud retrieval efforts, especially with the discrimination of cloud thermodynamic phase which is a critical component of the current study. As noted in Section 5.4, imperfect cloud phase discrimination can greatly increase the retrieval errors (lines 500-505).

Authors: This is a good suggestion but is unfortunately beyond this scope of this work. We will compare cloud property retrievals using CLARRA to CALIPSO in future work and thank the referee for this suggestion.

Referee: General comments: Lines 58-62: Two points to suggest here: 1. The authors point out the need for portable, low-cost, autonomous IR spectrometers that can make continuous measurements. But these measurements complement those from polar-orbiting IR spectrometers including IASI (on Metop-A/B/C), AIRS, and CrIS. It would be useful to provide an example where the surface measurements fill the gaps between satellite overpasses. 2. Additionally, a primary benefit to surface-based measurements is that the boundary layer is much better characterized than with profiles inferred from a satellite-based spectrometer. In particular, my impression is that the boundary layer profiles are much improved when temperature inversions are present, and this will impact the cloud properties if the layer is at/below the inversion.

Authors: This is a good point. We will add text such as the following to the introduction:

"Such measurements would be beneficial in a number of ways. They could be used to fill gaps in satellite measurements. For example, cloud properties were retrieved at Eureka from 2006 to 2009 from AERI measurements made nearly-continuously every ~40 seconds (Cox et al 2014). By contrast, satellite overpasses are typically twice per day. They can also be used to compare to satellite-based measurements. Finally, surface-based instruments are better at characterizing clouds in the boundary layer."

Referee: Section 3: This is a long section (over 6 pages) that discusses the Cloud and Atmo-spheric Radiation Retrieval Algorithm (CLARRA) in quite a bit of detail. Cloud height was discussed in great detail in Rowe et al. (2016) and is not repeated herein. Perhaps the readability would be improved by moving much of the theoretical development into an Appendix.

Authors: We have moved the theoretical development from Section 3.1 to the Appendix (almost 3 pages). To further improve readability, we have reorganized subsections in Section 3 and included the most important information in introductory paragraphs, making clear that the remainder of each section provides additional detail (which can be skipped).

Referee: Minor comments: Line 19: please define exactly what is meant by “mixed phase” - is it a homogeneous mixture of ice and liquid particles or something else?

Authors: Yes. We have clarified this: “Mixed-phase clouds were simulated as an external, homogeneous mixture of liquid and ice particles.”

Referee: The word “infrared” appears 26 times in the paper - could contract to IR

Line 47: include more up-to-date L’Ecuyer papers, e.g., “Reassessing the effect of cloud type on Earth’s energy balance in the age of active spaceborne observations. Part I: Top-of-atmosphere and surface”, by TS L’Ecuyer, Y Hang, AV Matus, Z Wang, in Journal of Climate, 2019. There is also a Part 2 manuscript in review.

Lines 293-294: Radiances are selected in two bands: 400 to 600 cm-1 and from 750to 1300 cm-1. As the method is using selected wavenumbers for each chosen spectral resolution, it would be useful to state them in this paper rather than in the supplemental.

Lines 340; 352; 557: suggest changing “in order to” to “to”

Line 356: change “found such error” to “found such errors”

Authors: Thank you - all of the above changes have been made.

Referee: Lines 503-505: Cloud height: is CO2 slicing used for both water and ice clouds? If so .... might want to change this so it’s used primarily for ice clouds and use 11-μm for optically thick clouds.

Authors: This is an interesting point but is beyond the scope of this work, which focuses more on the microphysical retrievals than the cloud height retrievals (discussed in Rowe et al 2016). We will investigate using 11 micron for cloud height retrievals in future work, and thank the reviewer for this suggestion.

Referee:

Line 536: Polar Regions does not have to be capitalized.

Line 561: suggest changing “correctable” to “mitigated”

Authors: We have made the above changes.

In addition to these changes and changes in response to the other reviewer, we have added a new figure (Fig. 4) and made a number of edits for grammar and clarity. We also made small

changes in the retrievals (e.g. standardized number of streams to 16, removed radiance error threshold); resulting differences are minor and do not affect our conclusions.

We thank the reviewer for these helpful suggestions that have improved our paper.

Toward autonomous surface-based infrared remote sensing of polar clouds: Retrievals of cloud microphysical properties

Penny M. Rowe[1,2], Christopher J. Cox[3,4], Steven Neshyba[5] and Von P. Walden[6]

[1]NorthWest Research Associates, Redmond, WA, USA.
[2]Department of Physics, Universidad de Santiago de Chile, Santiago, Chile.
[3]Cooperative Institute for Research in Environmental Sciences, University of Colorado, Boulder, USA.
[4]NOAA Earth System Research Laboratory, Physical Sciences Division, Boulder, USA.
[5]Chemistry Department, University of Puget Sound, Tacoma, USA.
[6]Department of Civil and Environmental Engineering, Washington State University, Pullman, USA

Correspondence to: Penny M. Rowe (penny@nwra.com)

Penny Rowe 8/20/2019 9:42 AM
Deleted: CO,

Penny Rowe 8/20/2019 9:42 AM
Deleted: Colorado, CO,

Penny Rowe 8/20/2019 9:42 AM
Deleted: WA,

Penny Rowe 8/20/2019 9:42 AM
Deleted: WA,

Abstract

Improvements to climate model results in polar regions require improved knowledge of cloud microphysical properties. Surface-based infrared (IR) radiance spectrometers have been used to retrieve cloud microphysical properties in polar regions, but measurements are sparse. Reductions in cost and power requirements to allow more widespread measurements could be aided by reducing instrument resolution. Here we explore the effects of errors and instrument resolution on cloud microphysical property retrievals from downwelling IR radiances for resolutions of 0.1 to 20 cm^{-1}. Retrievals are tested on 336 radiance simulations characteristic of the Arctic, including mixed-phase, vertically inhomogeneous, and liquid-topped clouds and a variety of ice habits. Retrieval accuracy is found to be unaffected by resolution from 0.1 to 4 cm^{-1}, after which it decreases slightly. When cloud heights are retrieved, errors in retrieved cloud optical depth (COD) and ice fraction are considerably smaller for clouds with bases below 2 km than for higher clouds. For example, at a resolution of 4 cm^{-1}, with errors imposed (noise and radiation bias of 0.2 mW/(m^2 sr cm^{-1}) and biases in temperature of 0.2 K and in water vapour of -3%), using retrieved cloud heights, root-mean-square errors decrease from 1.1 to 0.15 for COD, 0.3 to 0.18 for ice fraction (f_{ice}), and from 10 µm to 7 µm for ice effective radius (errors remain at 2 µm for liquid effective radius). These results indicate that a moderately low resolution, surface-based IR spectrometer could provide cloud property retrievals with accuracy comparable to existing higher resolution instruments, and that such an instrument would be particularly useful for low-level clouds.

Penny Rowe 8/20/2019 9:42 AM
Deleted: effect…ffects of errors and ... [1]

1 Introduction

Knowledge of polar cloud properties is critical for understanding climate change in polar regions. Polar regions are among the most rapidly warming regions on Earth, with significant concurrent changes in cloud properties that influence the amount of warming (Wang and Key 2005) and indications that sensitivity to clouds may increase in a warming Arctic (Cox et al 2015). Clouds have a strong influence on the polar surface energy budget (Lawson and Gettelman 2014; van den Broeke et al 2017), influencing sea ice loss (Francis and Hunter 2006; Kay et al 2009; Wang et al 2011) and Greenland ice melt (van den Broeke et al 2017). Despite ongoing efforts to improve cloud processes in climate models, the Intergovernmental Panel on Climate Change (IPCC) finds that "clouds and aerosols continue to contribute the largest uncertainty to estimates and interpretations of the Earth's changing energy budget," (Boucher et al, 2013). Improving the representation of cloud processes in climate models requires observational constraints, including ice and liquid water paths, particle size and thermodynamic phase (Komurcu et al 2014; Winker et al 2017). This is particularly true for the polar regions, where clouds and cloud processes are distinctly different from lower latitudes and present unique challenges for modeling cloud radiative effects (Hines et al 2004), and where measurements are sparse.

Penny Rowe 8/20/2019 9:42 AM
Deleted: surface-based
Penny Rowe 8/20/2019 9:42 AM
Deleted: challenging.

Although ground-based observations in the polar regions are sparse, measurements made during campaigns and at permanent field sites (e.g. Bromwich et al 2012; Cox et al 2014; Uttal et al., 2015, and references therein; Lachlan-Cope et al 2016; Silber et al 2018) and from satellites (e.g. L'Ecuyer and Jiang 2010) have made important contributions to our understanding of polar clouds. IR spectrometers are proven instruments for remote sensing that have been part of many of these surface and satellite-based measurements. Surface-based IR spectrometers are most sensitive to the cloud base, providing an important complement to satellite-based measurements. In particular, Atmospheric Emitted Radiance Interferometer (AERI) instruments currently operate at Barrow (1998-current), Eureka (2006-current), and Summit (June 2010-current): three Arctic Intensive Observing Sites (Uttal et al., 2015). In the Antarctic, there have been only short-term surface-based IR spectrometer measurements, including measurements made at Amundsen-Scott South Pole Station in 1992 (Mahesh et al 2001) and 2001 (Rowe et al 2008), at Dome C during Austral summer 2003 (Walden et al 2005) and 2012-2014 (Palchetti et al 2015), and McMurdo (as part of the Atmospheric Radiation measurement (ARM) West Antarctic Radiation Experiment, or AWARE; Silber et al 2018). These measurements are crucial, but represent only very sparse coverage of the polar regions.

Penny Rowe 8/20/2019 9:42 AM
Deleted: import
Penny Rowe 8/20/2019 9:42 AM
Deleted: Infrared
Penny Rowe 8/20/2019 9:42 AM
Deleted: the
Penny Rowe 8/20/2019 9:42 AM
Deleted: described above.
Penny Rowe 8/20/2019 9:42 AM
Deleted: infrared
Penny Rowe 8/20/2019 9:42 AM
Deleted: infrared

Because IR radiance measurements are passive, the energy requirements are considerably lower than for active instruments such as lidar. Thus there is the potential for portable, low-cost, autonomous IR spectrometers that could be deployed to remote locations to make widespread IR radiance measurements across the polar regions from which cloud microphysics could be retrieved. Such measurements would be beneficial in a number of ways: First, they could be used to fill gaps in satellite measurements. For example, cloud properties were retrieved at Eureka from 2006 to 2009 from AERI measurements made nearly continuously every ~40 seconds (Cox et al. 2014). By contrast, satellite overpasses are typically twice per day. Second, surface-based measurements can be used to validate satellite-based measurements. Finally, surface-based instruments are generally better at characterizing clouds in the boundary layer. To demonstrate the feasibility of such an instrument, the limitations of the retrieval given instrument operational constraints and availability of ancillary data must first be assessed.

Penny Rowe 8/20/2019 9:42 AM
Deleted: infrared
Penny Rowe 8/20/2019 9:42 AM
Deleted: infrared
Penny Rowe 8/20/2019 9:42 AM
Deleted: infrared

In this paper, we explore the accuracy with which cloud properties could be retrieved from a portable IR spectrometer, including optical depth, thermodynamic phase, and effective radius. This paper builds on similar work that explored the accuracy of cloud height retrievals (Rowe et al. 2016). One way to develop a robust, low-power portable spectrometer might be to reduce the instrument resolution. Here we quantify cloud-property retrieval accuracy as resolution becomes coarser, from 0.1 cm^{-1} to 20 cm^{-1}. Cloud properties are retrieved from simulated downwelling radiance spectra using the CLoud and Atmospheric Radiation Retrieval Algorithm (CLARRA). In addition to retrieving cloud height (Rowe et al. 2016), CLARRA retrieves cloud microphysical properties from IR radiances using an optimal inverse method in a Bayesian framework. Cloud property retrievals are performed for simulated polar clouds with varying atmospheric thermal and humidity structure, cloud optical depth (in the geometric limit; hereafter, COD), thermodynamic phase (including mixed-phase and supercooled liquid), liquid effective radius, ice effective radius, ice crystal habit, and cloud vertical structure.

Penny Rowe 8/20/2019 9:42 AM
Deleted: infrared
Penny Rowe 8/20/2019 9:42 AM
Deleted: 8
Penny Rowe 8/20/2019 9:42 AM
Deleted:), which uses
Penny Rowe 8/20/2019 9:42 AM
Deleted: (
Penny Rowe 8/20/2019 9:42 AM
Deleted: cloud optical depth or

Mixed-phase clouds were simulated as an external, homogeneous mixture of liquid and ice particles. We also examine the sensitivity of retrieved results on noise and bias imposed on the radiance, as well as on errors in specified input parameters, especially the atmospheric state and cloud height.

2 Simulated Radiances

To test the effect of instrument resolution on the ability to retrieve cloud properties from downwelling radiances, retrievals using CLARRA were performed on a set of simulations. Using simulations rather than actual measurements confers a variety of benefits: 1) the basic capability of the model, in the absence of error, can be determined, setting a benchmark for retrieval capability, 2) the effects of various sources of error (such as noise, bias, or uncertainty in the atmospheric state) can be determined and assessed independently, and 3) errors in the retrieved values are known and thus can be compared to assess the uncertainty prediction from the CLARRA model.

The set of simulated downwelling radiances is described in detail by Cox et al. (2016) and by Rowe et al (2016). The simulations are based on observed Arctic atmospheric profiles and cloud properties meant to represent a typical Arctic year, based on statistics from field observations (Cox et al. 2016 and references therein; although designed for the Arctic, significant overlap is expected for typical Antarctic atmospheric states, except perhaps in winter in the interior, when the atmosphere is colder and drier). All clouds were modeled as plane-parallel, single-layer clouds. Precipitable water vapour (PWV) varied from 0.2 to 3 cm.

A base set of 222 simulated radiances was created for atmospheres with vertically uniform clouds, using spheres for ice crystal habit (as well as for liquid droplet shape). Cloud bases vary from 0 to 7 km, with about 70% of clouds within the lowest 2 km and 30% above; thickness varies from 0.1 to 1.6 km; and temperatures vary from 225 to 282 K. Mixed-phase clouds are modeled as externally mixed and span temperatures of 240 to 273 K. Cloud phase includes liquid-only (~1/6 of cases), ice-only (~1/6) and mixed-phase (~2/3). Statistics for cloud microphysical properties are summarized in Table 1 (Statistics were generated for log-normal distributions of COD and effective radii. Thus the standard deviations were computed for the logarithms. For convenience, these were converted to positive and negative linear deviations in Table 1.)

A second set of simulated radiances was created for testing the effects of cloud vertical inhomogeneity, including 23 cases from the base set for which the cloud spanned multiple layers of the atmospheric model; these are referred to as "diffuse." Simulations were created for identical conditions, including the total COD, except that clouds were modeled as dense (physically thinner), inhomogeneous (the cloud was optically thicker at the center and thinner at the upper and lower edges), or liquid-topped (liquid cloud was confined to the uppermost layer, while ice cloud was confined to the lower model layers).

A third set was created for testing the effect of ice habit on the retrieval, including 9 base cases having an ice COD greater than 0.5. Simulations were created for identical conditions, except that single scattering properties from different cloud habits were used: hollow bullet rosettes, smooth plates, rough plates, smooth solid columns, and rough solid columns (Yang et al. 2005; 2013).

Penny Rowe 8/20/2019 9:42 AM
Deleted: used to test the retrieval

Penny Rowe 8/20/2019 9:42 AM
Deleted:), and are thus described only briefly here.

Penny Rowe 8/20/2019 9:42 AM
Deleted: simplistic clouds

Penny Rowe 8/20/2019 9:42 AM
Deleted: ; these clouds are

Penny Rowe 8/20/2019 9:42 AM
Deleted: and use

Penny Rowe 8/20/2019 9:42 AM
Deleted: (statistics

Penny Rowe 8/20/2019 9:42 AM
Deleted:).

Penny Rowe 8/20/2019 9:42 AM
Deleted: .

Penny Rowe 8/20/2019 9:42 AM
Deleted: 92 cases

Penny Rowe 8/20/2019 9:42 AM
Deleted: used to test

Penny Rowe 8/20/2019 9:42 AM
Deleted: . To do this,

Penny Rowe 8/20/2019 9:42 AM
Deleted: were selected

Penny Rowe 8/20/2019 9:42 AM
Deleted: then

Penny Rowe 8/20/2019 9:42 AM
Deleted: atmospheric and cloud

Penny Rowe 8/20/2019 9:42 AM
Deleted: that were identical

Penny Rowe 8/20/2019 9:42 AM
Deleted: of 54 cases

Penny Rowe 8/20/2019 9:42 AM
Deleted: used to test

Penny Rowe 8/20/2019 9:42 AM
Deleted: . For this purpose,

Penny Rowe 8/20/2019 9:42 AM
Deleted: were selected

Penny Rowe 8/20/2019 9:42 AM
Deleted: geometric optical depth

Penny Rowe 8/20/2019 9:42 AM
Deleted: atmospheric and cloud

Penny Rowe 8/20/2019 9:42 AM
Deleted: that were identical

The set of simulated spectra were created at monochromatic, or perfect resolution using the discrete ordinates radiative transfer model (DISORT; Stamnes et al 1988), with monochromatic gaseous optical depths created using the Line-By-Line Radiative Transfer Model (LBLRTM; Clough et al 2005) as inputs. Spectra were then convolved with a sinc function to obtain sets of spectra at resolutions of 0.1, 0.5, 1, 2, 4, 8 and 20 cm^{-1}. These are hereafter referred to as the "observed" spectra. Figure 1a shows a spectrum at 0.5 cm^{-1} resolution, together with the clear-sky spectrum for the same atmospheric conditions. Additional examples at 0.5 cm^{-1}, as well as at 4.0 cm^{-1}, are given in Fig. 2 of Rowe et al (2016).

3 CLoud and Atmospheric Radiation Retrieval Algorithm (CLARRA)

CLARRA retrieves cloud macrophysical properties (cloud height and temperature) and microphysical properties, (COD, ice fraction, effective radius of liquid droplets, and effective radius of ice crystals) from downwelling IR radiances, given knowledge of the atmospheric state. As the first step in the retrieval, cloud heights are retrieved by CLARRA as described by Rowe et al. (2016; see also references therein). Alternatively, cloud heights can be input into CLARRA (e.g. from other instrumentation, such as lidar, or from reanalysis models). Next, CLARRA performs a fast preliminary retrieval to estimate cloud microphysical properties (Section 3.1). These are then used as first-guess values in a microphysical retrieval that using uses an iterative optimal nonlinear inverse method (Section 3.2).

In preparation for running CLARRA, model atmosphere layer boundaries must be chosen and the atmospheric profiles must be constructed (based on model and measured data for the location and time of the downwelling radiance spectrum). For this work, the same atmospheric profiles used to create the simulated radiances are used (although errors are sometimes added). In addition to uncertainty estimates for the observed radiance, the microphysical retrieval requires *a priori* values for the microphysical properties and their covariance matrix. These can be taken from a climatology or can be determined from the fast retrieval. In this work, the statistics of the cloud properties used to create the simulated radiances are used. Finally, the observed spectrum and associated covariance matrix are needed (here, the simulated radiances with known errors are used). After these preparations, CLARRA is run as follows.

1. Compute gaseous layer optical depths at monochromatic resolution.
2. Using the above and the temperature profile, calculate terms related to emission and transmission by gases at the effective instrument resolution.
3. Retrieve cloud height (see Rowe et al 2016), or alternatively, input the cloud height from another source.
4. Perform the fast retrieval that neglects scattering, to get first-guess microphysical properties.
5. Perform the optimal iterative inverse method to retrieve cloud microphysical properties, using the first-guess or previous iteration results, the *a priori* and covariance matrix for the microphysical properties, and the observed spectrum and its covariance matrix.
6. Repeat step 5 until the result converges or a maximum number of iterations is reached.

For step 1, gaseous layer optical depths are computed at monochromatic resolution using LBLRTM. The cloud height retrieval (step 3) was described by Rowe et al (2016). The fast retrieval (step 4), the optimal inverse method (steps 5 and 6), and calculation of necessary terms (step 2) are described below.

Penny Rowe 8/20/2019 9:42 AM
Deleted: Infrared spectrometers operate at finite, rather than line-by-line, or perfect resolution. To determine the effect of reduced resolution on the cloud microphysical retrievals, resolutions of 0.1, 0.5, 1, 2, 4 and 8 cm^{-1} were tested. To mimic finite-resolution measurements, the

Penny Rowe 8/20/2019 9:42 AM
Deleted: , which

Penny Rowe 8/20/2019 9:42 AM
Deleted: perfect resolution, were

Penny Rowe 8/20/2019 9:42 AM
Deleted: each resolution. ... [2]

Penny Rowe 8/20/2019 9:42 AM
Deleted: cloudy-sky radiance

Penny Rowe 8/20/2019 9:42 AM
Deleted: .

Penny Rowe 8/20/2019 9:42 AM
Moved (insertion) [1]

Penny Rowe 8/20/2019 9:42 AM
Deleted: droplets) from downwelling infrared radiances, given knowledge of the atmospheric state.

Penny Rowe 8/20/2019 9:42 AM
Deleted: ... [3]

Penny Rowe 8/20/2019 9:42 AM
Moved up [1]: from other instrumentation, such as lidar, or from reanalysis models).

Penny Rowe 8/20/2019 9:42 AM
Deleted: Next, CLARRA computes the cloud emissivity, neglecting scattering, and retrieves from it first-guess estimates of cloud microphysical properties. Finally, the microphysical retrieval is performed using an iterative optimal nonlinear inverse method (Rodgers et al. 2000).

Penny Rowe 8/20/2019 9:42 AM
Deleted: dowelling

Penny Rowe 8/20/2019 9:42 AM
Deleted: ... [4]

Penny Rowe 8/20/2019 9:42 AM
Deleted: Retrieve

Penny Rowe 8/20/2019 9:42 AM
Deleted: for

Penny Rowe 8/20/2019 9:42 AM
Deleted: next

Penny Rowe 8/20/2019 9:42 AM
Deleted: using the current retrieval ... [5]

Penny Rowe 8/20/2019 9:42 AM
Deleted: the Line-By-Line Radiative ... [6]

Penny Rowe 8/20/2019 9:42 AM
Deleted: ; Clough

Penny Rowe 8/20/2019 9:42 AM
Deleted: 2005). Remaining

3.1 Fast preliminary retrieval

The preliminary retrieval provides a computationally fast estimate of cloud properties. Cloud properties are retrieved from the absorption optical depth, computed from the cloud emissivity, ignoring scattering. The fast retrieval can be used to inform real-time decisions about measurements (e.g. duration of time to averaging spectra for noise reduction) as well as providing estimates of cloud property statistics that can inform further analysis. Cloud properties retrieved from the fast retrieval also serve as a first guess for the iterative optimal inverse method described in the following section, with the goal of enhancing performance by starting iterations closer to the solution. Optionally, the fast retrieval results can provide input statistics for the optimal inverse method (a priori means and standard deviations). The description of the fast retrieval, below, can be skipped without loss in continuity.

The cloud emissivity is approximated as in Rowe et al (2016)

$$\varepsilon = \frac{R_{obs} - R_{clr}}{B_c t_c + R_c - R_{clr}}, \qquad (1)$$

where R_{obs} is the observed radiance, R_{clr} is the clear-sky radiance, B_c is the Planck function of cloud temperature, t_c is the surface-to-layer transmittance, and R_c is the surface-to-layer clear-sky radiance. All terms must be at the effective instrument resolution (as will be discussed in Sect. 3.3 and the appendix).

The cloud reflectivity is ignored so that the emissivity is assumed to be one minus the cloud transmittance. The natural logarithm of the cloud transmittance is the cloud absorption optical depth, which can thus be calculated from quantities that are measured or can be calculated independently of the cloud microphysical properties:

$$\tau_{a,obs} = -\ln\left(1 - \frac{R_{obs} - R_{clr}}{B_c t_c + R_c - R_{clr}}\right). \qquad (2)$$

The value of τ_a can also be calculated from the state variables: COD (τ_g), ice fraction (f_{ice}), effective radius of liquid (r_{liq}), and effective radius of ice (r_{ice}),

$$\tau_a = \tau_g/2\ [\ [1-f_{ice}]\ Q_{a,liq}(r_{liq}) + f_{ice}\ Q_{a,ice}(r_{ice})\ ]. \qquad (3)$$

$Q_{a,liq}$ and $Q_{a,ice}$ are the absorption efficiencies of liquid and ice, determined from the extinction efficiencies Q_e and the single scatter albedos ω_0. For ice

$$Q_{a,ice} = Q_{e\_ice}(r_{ice})\ [1-\omega_{0,ice}], \qquad (4)$$

where $Q_{e,ice}$ and $\omega_{0,ice}$ are determined for averages over a log-normal distribution of particle radii corresponding to the effective radius r_{ice}. For the fast preliminary retrieval, spheres were assumed for ice and single scattering parameters for each particle radius were calculated from Mie theory using the index of refraction of Warren et al (2008), based on a temperature

Penny Rowe 8/20/2019 9:42 AM
Moved (insertion) [2]

Penny Rowe 8/20/2019 9:42 AM
Deleted: **Resolution and Model E** ... [7]

Penny Rowe 8/20/2019 11:01 AM
Formatted: Right: 0.26"

Penny Rowe 8/20/2019 9:42 AM
Moved down [3]: the atmosphere is divided into model atmospheric layers and the approximation is made that the Planck function varies linearly with optical depth through the layer (Wiscomb et al 1976, Clough et al 1992). In the absence of scattering, the downwelling radiance from a layer at a given wavenumber is approximated as

Penny Rowe 8/20/2019 9:42 AM
Moved down [6]: $\widetilde{B}$ is the Planck function and θ is the viewing angle from zenith. ... [11]

Penny Rowe 8/20/2019 9:42 AM
Moved down [19]:). Following this, transmittances below 10^{-40} and above 1 were modified such that $10^{-40} <= t_L <= 1$.

Penny Rowe 8/20/2019 10:13 AM
Deleted: the atmosphere is divided into divided into model atmospheric layers and the approximation is made that the Planck function varies linearly with optical depth through the layer (Wiscomb et al 1976, Clough et al 1992). In the absence of scattering, the downwelling radiance from a layer at a given wavenumber is approximated as ... [8]

Penny Rowe 8/20/2019 9:42 AM
Moved down [4]: ... [9]

Penny Rowe 8/20/2019 9:42 AM
Deleted: effective-resolution transmittances can be greater than 1 or less than 0, res ... [12]

Penny Rowe 8/20/2019 9:42 AM
Deleted: Finally, since DISORT is run at single precision, serious errors can res ... [13]

Penny Rowe 8/20/2019 9:42 AM
Moved up [2]: **<#>Fast preliminary retrieval**

Penny Rowe 8/20/2019 9:42 AM
Deleted: **<#>: The first-guess** ... [14]

Penny Rowe 8/20/2019 9:42 AM
Formatted ... [10]

Penny Rowe 8/20/2019 9:42 AM
Deleted: $\tau = -\ln\left(1 - \frac{R_o - R}{\dots}\right.$ ... [15]

Penny Rowe 8/20/2019 9:42 AM
Deleted: (13

Penny Rowe 8/20/2019 9:42 AM
Deleted: (14

of 266 K. For liquid, single-scattering parameters determined from temperature-dependent indices of refraction at temperatures of 240, 253, 263, and 273 K were used (Rowe et al 2013; Zasetsky et al 2005; Wagner et al 2005). Letting T_1 be the temperature from this list that is closest to but lower than the cloud temperature, and T_2 be the temperature closest to but higher than the cloud temperature, $Q_{a,liq}$ is given as the weighted sum

$$Q_{a,liq} = w_1\, Q_{e\_liq}(r_{liq},T_1)\,[1-\omega_{0,liq}\,(r_{liq},T_1)] + w_2\, Q_{e\_liq}(r_{liq},T_2)\,[1-\omega_{0,liq}\,(r_{liq},T_1)] \qquad (5)$$

where $w_1 = (T_2 - T_c)/\,(T_2 - T_1)$ and $w_2 = (T_c - T_1)/\,(T_2 - T_1)$.

The values of $Q_{e,liq}$ and $Q_{e,ice}$, $\omega_{0,liq}$, and $\omega_{0,ice}$, are pre-computed for the full range of possible r_{liq} and r_{ice}. The COD (τ_g) is retrieved by inverse retrieval (using Eqs. (6) and (7) below, but with **R** replaced with $\tau_{a,obs}$, **F** replaced with Eq. (3) and $\gamma = 0$). Next, $\tau_{a,obs}$ is calculated for the retrieved τ_g and for a variety of values of f_{ice}, (0.2, 0.4, 0.6, 0.8), r_{liq} (integers between 5 and 30) and r_{ice} (even numbers between 10 and 50). Calculating $\tau_{a,obs}$ for all combinations of these values is computationally fast compared to other aspects of CLARRA. Finally, the values of f_{ice}, r_{liq}, and r_{ice} are selected that correspond to the minimum absolute difference between $\tau_{a,obs}$ and τ_a.

3.2 Optimal Nonlinear Inverse Method

The optimal nonlinear inverse method iteratively retrieves cloud microphysical properties (COD, f_{ice}, r_{liq}, and r_{ice}), using the results of the fast retrieval as a first guess. The inverse method uses radiances from 400 to 600 cm^{-1} (allowing thermodynamic phase determination; Rathke et al. 2002a) and from 750 to 1300 cm^{-1}, which is sensitive to phase, COD and effective radius. Similar optimal nonlinear inverse methods have been used to retrieve cloud properties from AERI instruments in the Arctic (Turner 2005; Cox et al 2014) and from satellite instruments (L'Ecuyer et al 2006; Wang et al 2006; Poulsen et al., 2012; L'Ecuyer et al 2006). Cloud properties are retrieved from observed radiances averaged in microwindows (see Table 2). The remainder of this section provides additional details about the optimal nonlinear inverse method.

The inversion equation used here is the iterative Levenberg-Marquardt method (Rodgers 2000 and references therein),

$$\mathbf{x}_{i+1} = \mathbf{x}_i + \left\{\left[1+\gamma_i\right]\mathbf{S}_a^{-1} + \mathbf{K}_i^T\mathbf{S}_e^{-1}\mathbf{K}_i\right\}^{-1}\left\{\mathbf{K}_i^T\mathbf{S}_e^{-1}\left[\mathbf{R}-\mathbf{F}(x_i)\right]-\mathbf{S}_a^{-1}\left[\mathbf{x}_i-\mathbf{x}_a\right]\right\}, \qquad (6)$$

where **x** is the state vector, with *a priori* $\mathbf{x}_a$ and covariance matrix $\mathbf{S}_a$. The subscript *i* indicates the iteration number and **R** is the observation, with covariance matrix $\mathbf{S}_e$. **F** is the forward model (described below), and the kernel (**K**) is the Jacobian matrix, computed numerically by perturbing each state variable in turn and re-running **F**.

The Levenberg-Marquardt formulation is a hybrid of the Gauss-Newton formulation and the method of steepest descent, with $\gamma = 0$ defaulting to Gauss-Newton. As γ increases, Eq. (6) becomes more heavily weighted towards steepest descent and convergence slows. Choosing γ is difficult, as a large value of γ will slow the retrieval. Here we start with $\gamma = 0$. Each

Penny Rowe 8/20/2019 9:42 AM
Deleted: Both spherical and realistic ice habits were used in the full retrieval. Scattering properties for hollow bullet rosettes and smooth and rough solid columns and plates were provided by Yang et al (2013).

Penny Rowe 8/20/2019 9:42 AM
Deleted: (15

Penny Rowe 8/20/2019 9:42 AM
Deleted: 16…) and (17) given…) be ... [16]

Penny Rowe 8/20/2019 9:42 AM
Deleted: The optimal nonlinear

Penny Rowe 8/20/2019 9:42 AM
Deleted: The optimal nonlinear…he ... [17]

Penny Rowe 8/20/2019 9:42 AM
Deleted: $\mathbf{x}_{i+1} = \mathbf{x}_i + \left\{\left[1+\gamma_i\right]\mathbf{S}^{-1} + \mathbf{K}^T$ ... [18] , (16)

Penny Rowe 8/20/2019 11:01 AM
Formatted: Right: 0.26"

Penny Rowe 8/20/2019 9:42 AM
Formatted: Font:Bold

Penny Rowe 8/20/2019 9:42 AM
Deleted: is S_a.

Penny Rowe 8/20/2019 9:42 AM
Formatted: Font:Not Italic

Penny Rowe 8/20/2019 9:42 AM
Deleted: observed radiance spectrum

Penny Rowe 8/20/2019 9:42 AM
Formatted: Font:Not Italic

Penny Rowe 8/20/2019 9:42 AM
Deleted: The… is the forward model ... [19]

Penny Rowe 8/20/2019 9:42 AM
Deleted: $K(x_1) = \frac{R(x_1,x_2,...)-R'(x_1'}{x_1 - x_1'}$ (17

Penny Rowe 8/20/2019 9:42 AM
Moved down [20]:)
where

Penny Rowe 8/20/2019 9:42 AM
Deleted: primes indicate that a perturbation was applied. After computing **K** for each x_i, these are combined into a matrix with rows K(x_1), K(x_2), etc. ... [20]

Penny Rowe 8/20/2019 9:42 AM
Formatted: Not Superscript/ Subscript

Penny Rowe 8/20/2019 9:42 AM
Deleted: = 0. If

time the current iteration causes the root-mean-square (rms) error between measurement and forward model result to increase in magnitude by more than 1 RU, or by more than double the current error, γ is increased (first to γ = 1 and then) by a factor of 10; the retrieval is then repeated with the new γ. After increasing γ, if a subsequent iteration does not increase the rms error as described above, γ is decreased by a factor of 10. Iterations are repeated until γ < 0.01 or the maximum allowed number of iterations is reached.

Error in the retrieved state variable is given by the covariance matrix

$$\mathbf{S} = (\mathbf{K}^T\mathbf{S}_e^{-1}\mathbf{K} + \mathbf{S}_a^{-1})^{-1} \qquad (7)$$

Note that this equation applies only when γ = 0. We find that our criterion of γ < 0.01 results in negligibly different retrievals than for γ = 0. Convergence is tested using

$$d_i^2 = (\mathbf{x}_i - \mathbf{x}_{i+1})^T\mathbf{S}^{-1}(\mathbf{x}_i - \mathbf{x}_{i+1}) \ll n, \qquad (8)$$

(Rodgers 2000), where n is the length of $\mathbf{x}$.

In this work, the "observation" **R** is derived from the simulated spectra described in Sect. 2 by averaging radiances in microwindows between strong gaseous emission lines. Microwindows used in this work for resolutions of 0.1 to 4 cm^{-1} are shown in Table 2. They span 3-10 cm^{-1} and include at least one radiance (wavenumber spacing is equivalent to resolution). For retrievals at 8 and 20 cm^{-1}, the closest measurement point to each central microwindow frequency was used. Using radiances in microwindows minimizes the contribution by gases, increasing sensitivity to cloud and reducing errors. However, due to the finite resolution, gas emission from outside the microwindow is convolved into radiances within the microwindow. For example, at a resolution of 0.1 cm^{-1}, in a microwindow of 4 cm^{-1}, the contribution from gaseous absorption lines outside the microwindow will be minimal. As resolution gets coarser, the gaseous absorption lines bordering the microwindow contribute more and more, potentially decreasing sensitivity and increasing errors.

The state vector **x** is composed of COD, ice fraction, log of the effective radius of liquid, and log of the effective radius of ice, so that n = 4. For the *a priori* ($\mathbf{x}_a$), means of the values of **x** used to create the base set are used (Table 1). The covariance matrix $\mathbf{S}_a$ is assumed to be diagonal, with diagonal elements based on a standard deviation of about one half the range of values; this is used rather than using the standard deviations given in Table 1 to weight the retrieval heavily toward the measurement rather than the *a priori*. The error covariance matrix for radiance ($\mathbf{S}_e$) is assumed to be diagonal with elements based on the model errors described in the next section and the measured and simulated radiance errors due to any imposed errors, added in quadrature. The first guess values (i = 0) are determined from the fast microphysical property retrieval. The maximum number of allowed iterations was set to 20 and the tolerance for convergence was set to $d^2 < 1$. For convenience, the result of the forward model acting on the retrieved state vector is termed the retrieved radiance.

The forward model (**F**) is calculated by running DISORT with the state variables and with effective-resolution gaseous optical depths (described below). Other inputs to DISORT include the solar contribution, surface albedo, temperature profile, and the Legendre moments that describe the phase function, single-scatter albedo, and COD, which depend on the

Penny Rowe 8/20/2019 9:42 AM
Deleted: first

Penny Rowe 8/20/2019 9:42 AM
Deleted: error

Penny Rowe 8/20/2019 9:42 AM
Deleted: by more than a specified threshold,

Penny Rowe 8/20/2019 9:42 AM
Deleted: γ_I = 1. For following iterations,

Penny Rowe 8/20/2019 9:42 AM
Deleted: increases more than the threshold, γ_{i+1} is increased to 10 γ_i, while if it doesn't, γ_{i+1}

Penny Rowe 8/20/2019 9:42 AM
Deleted: to 0.1 γ_i.

Penny Rowe 8/20/2019 9:42 AM
Deleted: $_i$

Penny Rowe 8/20/2019 9:42 AM
Deleted: and convergence is achieved,

Penny Rowe 8/20/2019 9:42 AM
Deleted: until

Penny Rowe 8/20/2019 9:42 AM
Deleted: The error threshold was set by trial and error to be an increase in magnitude of the rms error between measurement and forward model by more than 1 RU or by more than double the current rms error.

Penny Rowe 8/20/2019 9:42 AM
Deleted: , (18

Penny Rowe 8/20/2019 9:42 AM
Deleted: and convergence

Penny Rowe 8/20/2019 9:42 AM
Deleted: (19

Penny Rowe 8/20/2019 9:42 AM
Deleted: 2 by averaging the simulated radiances in the microwindows. Selected microwindows (see Supplemental) are similar to those in Turner (2005) and Garrett and Zhao (2013). Microwindows typically span at least 4 cm^{-1}, so that at least one simulated radiance falls in each microwindow, e ... [21]

Penny Rowe 8/20/2019 9:42 AM
Deleted: true

Penny Rowe 8/20/2019 9:42 AM
Deleted: in order

Penny Rowe 8/20/2019 9:42 AM
Formatted: Font:Not Italic

Penny Rowe 8/20/2019 9:42 AM
Deleted: previous

Penny Rowe 8/20/2019 9:42 AM
Formatted: Font:Bold

Penny Rowe 8/20/2019 9:42 AM
Deleted: the

Penny Rowe 8/20/2019 9:42 AM
Deleted: previously as input.

state variables and cloud height. DISORT is run with 16 streams. Single scattering properties were the same as for the fast preliminary retrieval.

3.3 Resolution and Model Errors

In this work, DISORT was used both for simulating the "observed" radiances and for the forward model **F**. DISORT requires gaseous layer optical depths, which are calculated more accurately for observed radiances compared to those used in **F**. Gaseous layer optical depths computed by LBLRTM are at monochromatic, or perfect resolution and a fine wavenumber spacing, and DISORT must be run for each wavenumber, after which the radiance must be convolved to instrument resolution. This was done to simulate the observations but is too computationally intensive for the iterative inverse retrieval (i.e. for **F**). Instead, we develop a novel method for producing effective-resolution gaseous layer optical depths (given in the Appendix) so that DISORT need only be run for each microwindow.

Model errors arising from these differences are shown in Fig 1b, as box and whiskers plots of model errors for cloudy-sky radiances at 0.5 cm^{-1} resolution, in microwindows used in the cloud microphysical property retrievals. The errors were calculated as differences between downwelling radiances calculated using the effective-resolution layer optical depths (described in the Appendix) and monochromatic radiances convolved with the instrument lineshape (the radiance simulations described in Sect. 2), and averaged in microwindows. At 0.5 cm^{-1} resolution, median model errors are within +/- 0.02 RU (1 RU = 1 $mW/(m^2\ sr\ cm^{-1})$). For resolutions of 0.1 to 2 cm^{-1}, all model errors are within +/- 0.15 RU (figures for other resolutions are given in the Supplemental). For resolutions of 4 to 20 cm^{-1}, model errors generally increase with coarsening resolution, with maximum errors of -0.7 to 1.0 RU at 20 cm^{-1} resolution (Supplemental).

Another source of model error is related to the cloud height retrieval. The cloud height retrieval also uses effective-resolution terms: the gaseous radiance and the transmittance from the surface up to each possible cloud layer (R_c and t_c), and the clear-sky radiance (R_{clr}), described in Rowe et al (2016). Derivation of these quantities is given in the Appendix. Model errors for a typical clear-sky radiance used in the cloud height retrievals are also shown in Fig. 1b (solid blue curve); the error shown is the difference between R_{clr} calculated in this work (as described in the Appendix) and the monochromatic radiance from LBLRTM convolved with the instrument lineshape. As the figure shows, model errors for clear skies are typically very low.

4 Imposed Errors

To determine the impact of sources of error on the microphysical retrievals, various errors were imposed on "observed" radiances, including Gaussian noise (mean of 0.2 RU) and bias (± 0.2 RU). In remote locations, reanalysis datasets may be used for specification of the atmospheric state. Wesslen et al. (2014) characterized temperature errors in the European Centre for Medium-range Forecasting (ECMWF) Interim (ERA-Interim; Dee et al., 2011) as varying from -0.5 K to 1 K. Rowe et al (2016) found such errors to have a roughly equivalent effect on radiative transfer calculations as a positive temperature bias of 0.2 K. Wesslen et al. (2014) characterized water vapour errors to be 2% to 10%, with lower biases in the first 3 km and higher biases above. Because water vapour decreases rapidly with height, this was found to be roughly equivalent to a water vapour bias at all heights of 3% (Rowe et al 2016). Thus, imposed errors also included biases in the atmospheric temperature (± 0.2 K) and water vapour (± 3%). Higher biases in water vapour and temperature were also tested (± 10% and ± 1 K). Microphysical properties were retrieved with these errors each imposed in isolation, using both true

Penny Rowe 8/20/2019 9:42 AM
Deleted: In order to

Penny Rowe 8/20/2019 9:42 AM
Deleted: (±

Penny Rowe 8/20/2019 9:42 AM
Deleted: (

Penny Rowe 8/20/2019 9:42 AM
Deleted: error

Penny Rowe 8/20/2019 9:42 AM
Deleted: (Rowe et al 2016).

Penny Rowe 8/20/2019 9:42 AM
Deleted: vapor

Penny Rowe 8/20/2019 9:42 AM
Deleted: PWV

Penny Rowe 8/20/2019 9:42 AM
Deleted: PWV

Penny Rowe 8/20/2019 9:42 AM
Deleted: Based on this work

Penny Rowe 8/20/2019 9:42 AM
Deleted: errors

Penny Rowe 8/20/2019 9:42 AM
Deleted:),

Penny Rowe 8/20/2019 9:42 AM
Deleted: the precipitable

Penny Rowe 8/20/2019 9:42 AM
Deleted: vapor, or PWV

Penny Rowe 8/20/2019 9:42 AM
Deleted: In addition, higher errors

Penny Rowe 8/20/2019 9:42 AM
Deleted: PWV

Penny Rowe 8/20/2019 9:42 AM
Deleted: %).

cloud heights and cloud heights retrieved with CO_2 slicing as described in Rowe et al (2016).

In addition to errors imposed in isolation, various combinations of the above sources of errors were imposed on retrievals, as described in Sect. 5 below.

5 Results and Discussion

5.1 Retrieval overview

Use of the fast retrieval as a starting point for the inverse retrieval was found to have a variety of benefits. The fast retrieval reduced rms errors relative to the *a priori*: from 300% to 6% for τ_g, from 0.4 to 0.2 for f_{ice}, from 4.4 to 3.7 µm for r_{liq} and from 16 to 11 for r_{ice}. This provided a first-guess for the inverse retrieval that was closer to the solution, lowering retrieval errors slightly, modestly increasing the number of cases that converged, and preventing convergence to an incorrect solution for a few cases. Overall, the greatest improvement from using the fast preliminary retrieval was reducing computation time; on average, one fewer iteration was needed when the fast retrieval was used.

Figure 2 shows the inverse-retrieval trajectory, with iterations, for an ice-only cloud with a COD of 0.89 and effective radius of 22 µm. The retrieval trajectory is superimposed on error contours (root-mean-square radiance differences). As the figure shows, the retrieval converged from the first-guess value (red dot on right in each panel), to the minimum in 4 iterations. Furthermore, the retrieval correctly converged to an ice-only cloud, although the mean cloud temperature of ~256 K falls within the range of temperatures where mixed-phase clouds may occur.

Retrievals using the base set of simulations indicate that the kernels are typically sufficiently linear to converge on the solution, except for large COD and effective radii. We find that the retrievals lose sensitivity to COD between about 5 and 10 (see Sect. 5.2 below); in previous work retrieving cloud properties from downwelling IR radiances in a similar wavenumber range, cut-offs of 4 to 6 were used (Mahesh et al 2001; Rathke 2002a,b; Turner 2005). The retrievals were found to lose sensitivity to effective radius above about 50 µm (see Supplemental), which is in keeping with Rathke and Fischer (2000) and Garrett and Zhao (2013), but differs from the cut-off values of 25 µm used by Mahesh et al (2001) and of 100 µm by Turner (2005). In addition, when values approach these limits, the retrieval was found to sometimes move away from the solution. To avoid this, upper bounds were set for the COD (10) and effective radius (50 µm), and the kernels were typically calculated for a step in the direction of smaller COD and effective radius; that is, in the direction where sensitivity is larger.

Nearly all retrievals converged to within the specified tolerance in d^2, with only 0 to 2 cases failing to converge for any set of imposed errors. Overall, convergence was achieved in a mean of 4 iterations (median of 3). At most 2 cases failed to converge within 20 iterations for any set of imposed errors.

5.2 Retrieval Errors

To determine the retrieval capability, errors in retrieved values are examined in the absence of any imposed errors, where only model errors are present. Table 3 shows errors in retrieved cloud microphysical properties (τ_g, f_{ice}, r_{liq}, and r_{ice}) for the

Penny Rowe 8/20/2019 9:42 AM
Deleted: used: ... [22]

Penny Rowe 8/20/2019 11:01 AM
Formatted: Justified, Right: 0.26", Tabs: 6.75", Left

Penny Rowe 8/20/2019 11:01 AM
Formatted: Right: 0.26"

Penny Rowe 8/20/2019 11:01 AM
Formatted: Heading 2, Indent: Left: 0", Hanging: 0.4", Right: 0.26", Space Before: 12 pt, After: 12 pt

Penny Rowe 8/20/2019 10:17 AM
Formatted: Font:10 pt

Penny Rowe 8/20/2019 10:17 AM
Deleted: ... [23]

Penny Rowe 8/20/2019 11:01 AM
Formatted: Right: 0.26"

Penny Rowe 8/20/2019 9:42 AM
Deleted: error contours …he inverse ... [24]

Penny Rowe 8/20/2019 9:42 AM
Deleted: The radiative transfer loses ... [25]

Penny Rowe 8/20/2019 9:42 AM
Deleted: For retrievals performed for base cases for varying levels of imposed error, retrievals generally converged within 20 iterations (at…t most 2 cases failed to ... [26]

Penny Rowe 8/20/2019 9:42 AM
Deleted: The effect of using the fast retrieval result as a first guess was also examined. The fast retrieval was found to provide a first-guess value that is generally closer to the solution than the *a priori*. Compared to using the *a priori*, using the fast retrieval result as the first guess reduces the rms error in the first guess from 300% to 6% for τ_g, from 0.4 to 0.2 for f_{ice}, from 4.4 to 3.7 µm for r_{liq} and from 16 to 11 for r_{ice}. (The first-guess values for τ_g and r_{ice} were not allowed to exceed 5 and 50 µm, respectively). Use of the fast retrieval lowered retrieval errors slightly and modestly increased the number of cases that converged (typically an increase of no more than 1 case). In rare cases, using the fast retrieval can avoid spurious results with large errors due to incorrectly converging (this occurred one or fewer times for each set of retrievals). Overall, the greatest improvement from using the fast preliminary retrieval is computational speed. On average, one fewer iteration was needed when the fast retrieval was used.

Penny Rowe 8/20/2019 9:42 AM
Deleted: 2

base set of spectra, for spectral resolutions of 0.1, 0.5, and 4 cm^{-1}. Retrieval errors are shown for different ranges of τ_g. For thin clouds (τ_g < 0.4), the low signal reduces sensitivity. For thick clouds (τ_g > 5), the spectrum begins to approach saturation, and sensitivity to the cloud's microphysical properties diminishes. Both can result in large errors in f_{ice}, r_{liq}, and r_{ice} (such increases are not seen for τ_g > 5 in Table 3 but occur when errors are imposed). By contrast, error in τ_g increases with increasing τ_g and is smallest for the thinnest clouds. Based on these considerations, the ideal range for τ_g was identified as 0.4 < τ_g < 5. (To get a sense of how common such clouds are, Cox et al, 2014 found that at Eureka, Nunavut, in 2006-2009, clouds with optical depths of 0.25 to 6 accounted for about 32% of AERI measurements; 17% when quality control procedures and a PWV threshold of 1 cm were applied; in this work PWV is as high as 3 cm). Unless otherwise specified, results will be presented for this range. Retrieval errors for 0.4 < τ_g < 5 are overall quite low, with magnitudes of errors in τ_g below 0.013, in f_{ice} below 0.03, in r_{liq} below 0.7 µm, and in r_{ice} below 4 µm. Overall, the table shows no trend in retrieval errors with coarsening resolution for 0.4 < τ_g < 5.

Retrieval accuracy was tested for two sets of microwindows. Set 1 consists of 22 microwindows similar to those used by Turner (2005), indicated in Table 2 in plain (non-bold) font; these were used in the retrievals described below. Set 2 consists of the combined microwindows of Rathke et al (2000) and Mahesh et al (2001), indicated in Table 2 with superscripts R and M (11 microwindows). Retrieval errors were found to be slightly lower for set 1; therefore it is used in the remainder of this work. However, differences were small (compare Table 4, described below, to Table S1 of the Supplemental), indicating that a smaller set of microwindows is likely sufficient. Choice of optimal microwindows depends on noise level and spectrally-varying errors (e.g. due to errors in assumed profiles of atmospheric water vapour and chlorofluorocarbons) and is therefore a complicated but interesting topic for future work.

Errors in retrieved microphysical cloud properties for different imposed errors are given in Table 4 for a spectral resolution of 0.5 cm^{-1} and τ_g between 0.4 and 5. Magnitudes of imposed errors are given in the first column except for cases of combined errors. Error combination (a) includes noise of 0.2 RU, radiation bias of 0.2 RU, temperature bias of 0.2 K, and water vapour bias of -3%, and uses true cloud heights. Combination (b) is the same but with opposite signs on biases. Combinations (c) and (d) are the same as (a) and (b), respectively, but use retrieved cloud heights (similar sets but with radiation biases of 0.5 RU are given in Table S2 of the Supplemental). Subsequent columns give the mean errors and the standard deviations of the errors.

When true cloud heights are used, errors in τ_g are within ± 0.2 for large biases imposed on the observed radiation, temperature, and water vapour, (± 1.0 RU, 1 K, and 10%, respectively) or combined errors, and within ± 0.09 for smaller imposed biases (± 0.2 RU, 0.2 K, and 3% respectively). Large imposed errors also lead to large errors in f_{ice}, making it difficult to distinguish liquid and ice. Errors in r_{ice} are typically 2 to 3 times as large as errors in r_{liq}. Mean errors reveal how biases in measured radiance, water vapour and temperature lead to biases in retrieved cloud properties. For example, positive biases in observed radiances lead to negative biases in COD, r_{liq}, and r_{ice}, and positive biases in ice fraction, while the reverse is true for negative biases in observed radiance.

When cloud heights are retrieved from the observed radiances (columns labelled CO_2 slicing and combined errors (c) and (d)), errors in cloud height lead to biases in inferred cloud temperature. Biases in cloud temperature cause errors that are

Penny Rowe 8/20/2019 9:42 AM
Deleted: Results were omitted where the root-mean-square difference between observed and retrieved spectra was greater than 1 RU; this resulted in omitting a single point for 4 cm^{-1} resolution.

Penny Rowe 8/20/2019 9:42 AM
Deleted: -to-noise is low

Penny Rowe 8/20/2019 9:42 AM
Deleted: . (Error

Penny Rowe 8/20/2019 9:42 AM
Deleted: τ_g, by

Penny Rowe 8/20/2019 9:42 AM
Deleted:).

Penny Rowe 8/20/2019 9:42 AM
Deleted: 02

Penny Rowe 8/20/2019 9:42 AM
Deleted: 12

Penny Rowe 8/20/2019 9:42 AM
Deleted: 1.2

Penny Rowe 8/20/2019 9:42 AM
Deleted: 5. The

Penny Rowe 8/20/2019 9:42 AM
Deleted: a slight increase

Penny Rowe 8/20/2019 9:42 AM
Deleted: error

Penny Rowe 8/20/2019 9:42 AM
Deleted: , which is most pronounced

Penny Rowe 8/20/2019 9:42 AM
Deleted: f_{ice} and r_{liq}

Penny Rowe 8/20/2019 9:42 AM
Deleted: 3

Penny Rowe 8/20/2019 9:42 AM
Deleted: , which

Penny Rowe 8/20/2019 9:42 AM
Deleted: detailed in Sect. 4.

Penny Rowe 8/20/2019 9:42 AM
Deleted: means

Penny Rowe 8/20/2019 9:42 AM
Deleted: Cases are again omitted when the root-mean-square difference between the observed and retrieved radiance is greater than 1 RU; this resulted in 12, 9, and 2 points being removed for PWV biases of 10% and -10% and set d of combined errors (respectively).

Penny Rowe 8/20/2019 9:42 AM
Deleted: PWV bias (± 10%)

Penny Rowe 8/20/2019 9:42 AM
Deleted: 04 for all other imposed errors (one standard deviation).

Penny Rowe 8/20/2019 9:42 AM
Deleted:), biases imposed on radiation, temperature, and PWV cause biases in cloud temperature. The biases in cloud temp ... [27]

spectrally flat. Because cloud emissivity depends fairly linearly on τ_g, spectrally flat errors have a large effect on τ_g. Furthermore, in the cloud height retrieval (CHR), the cloud is placed in the atmospheric model layer containing the cloud height retrieved with CO_2 slicing. This means that errors in COD are also affected by the choice of atmospheric layering. One approach to improving cloud temperature and optical depth is the geometric method of Rathke et al (2002b), for which the instrument would be designed to look at multiple angles; this can also be used to examine the horizontal homogeneity of clouds.

Additional work is needed to understand the effects of CHR errors on microphysical property retrievals, for several reasons. First, Rowe et al (2016) found that CHR errors for CO_2 slicing were most sensitive to biases in observed radiance and temperature, with less sensitivity to noise and biases in water vapour. By contrast, for an alternate CHR method (MLEV) these sensitivities were found to be the opposite. Since CHR errors translate into errors in retrieved optical depth, it is important to choose the CHR method to use based on expected error magnitudes. Second, Rowe et al (2016; see e.g. Fig. 7) found that CHR errors generally decrease with increasing cloud signal, which should oppose the tendency of microphysical-property retrieval errors to grow with increasing optical depth. Finally, Rowe et al (2016; Fig. 7) found that CHR errors generally decrease with decreasing cloud height. Here we find important consequences for retrievals of COD and f_{ice}. For example, when errors are imposed (noise of 0.2 RU, radiation bias of 0.2 RU, temperature bias of 0.2 K, water vapour bias of -3%, and CHR errors in cloud height; for spectra at 4.0 cm^{-1} resolution), comparing clouds with based above 2 km to those with bases below, rms errors in retrieved COD decrease from 1.1 to 0.15, errors in f_{ice} decrease from 0.3 to 0.18, and errors in r_{ice} decrease from 10 to 7 µm (errors remain at 2 µm for the effective radius of liquid).

Errors in retrieved microphysical properties are shown as a function of resolution from 0.1 to 20 cm^{-1}, for clouds with bases below 2 km, in Fig. 3. Errors are shown for base cases with no imposed error and for a combination of imposed errors: noise of 0.2 RU, radiation bias of 0.2 RU, temperature bias of 0.2 K, water vapour bias of -3%, and CHR errors in cloud height. No trend is seen in retrieval errors for resolutions of 0.1 to 4 cm^{-1}, after which errors increase. For clouds with bases above 2 km, errors are larger for optical depth and ice fraction (Figure S4 of the Supplemental) and trends with resolution are similar but less pronounced. (Scatter plots of true vs retrieved microphysical properties are given in Figs. S5 and S6 of the Supplemental). Based on these trends, an instrument resolution of 4 cm^{-1} seems to be a good compromise for reducing resolution while avoiding increases in retrieval errors. For example, at 0.5 cm^{-1} (for clouds at all heights), rms retrieval errors are 0.6 for COD, 0.2 for f_{ice}, 3 µm for r_{liq}, and 8 µm for r_{ice}; at 4 cm^{-1} they are nearly the same (0.6, 0.2, 2 µm, and 8 µm, respectively).

5.3 Retrieval error covariance matrix

Discussion of errors so far has focused on actual retrieval errors, which can be calculated because simulated data was used as the observation set. For real measurements, error analysis relies on the covariance matrix **S**, which in turn depends on the kernels and covariance $\mathbf{S}_e$ (Eq. (8); $\mathbf{S}_e$ is calculated by adding measurement and forward model errors in quadrature; model errors are determined from errors in water vapour or temperature profiles). Here we determine how well **S** represents retrieval errors. For unbiased, normally distributed errors, the diagonals of **S** should correspond to the 68% confidence interval. We can test this by comparing retrieval errors to the diagonal of **S**. This is complicated by the fact that **S** is not constant but depends on **x** (because the kernels depend on **x**). Thus for each retrieved **x**, the absolute error was divided by the square root of the appropriate diagonal element of the corresponding **S**. For Gaussian errors, this ratio should be <=1 for

Penny Rowe 8/20/2019 9:42 AM
Deleted: so that …pectrally flat erro ... [28]

Penny Rowe 8/20/2019 9:42 AM
Deleted: uncertainties in retrieved r_{ice} for real…HR errors for CO_2 slicing were ... [29]

Penny Rowe 8/20/2019 9:42 AM
Deleted: state variables …icrophysic ... [30]

Penny Rowe 8/20/2019 9:42 AM
Moved down [21]: For

Penny Rowe 8/20/2019 9:42 AM
Deleted: comparison to Rowe et al (2016), retrieval errors were estimated for a surface-based infrared radiance spectrometer at 4 cm^{-1} resolution with a radiation bias of 0.2 RU and noise of 0.2 RU. Since reanalysis data would likely be used to characterize the atmospheric state, error estimates discussed previously were used for errors in temperature (bias of 0.2 K) and PWV (bias of 3%). (This is error combination h, described in Sect. 4). Furthermore, it was assumed that no independent data for cloud heights would be available, so cloud height was retrieved using CO_2 slicing. For the same cases and imposed errors, Rowe et al (2016) reported errors that increase from approximately 0.5 to 1.5 km as cloud-base height …ncrease ... [31]

Penny Rowe 8/20/2019 9:42 AM
Deleted: 18)). Recall that…); $\mathbf{S}_e$ dep ... [32]

68% of retrievals (and <=2 for 95% of retrievals, etc). In the absence of imposed error, only 52 to 63% of retrievals had a ratio within 1 (for $\mathbf{S}_e$ based on model errors). The lowest model errors are likely underestimates, since it is unlikely all sources of error in the forward model were captured. A minor increase in model error (0.03 RU) gave values between 68 and 77%. However, the error distributions were found to decrease more slowly than Gaussians, with only 78 to 87% of errors (rather than 94%) falling within the second standard deviation indicated by **S**.

For imposed noise of 0.2 RU, only 52 to 58% of retrievals were found to have a ratio within 1, suggesting that model errors are amplified in the presence of error. This is likely because away from the correct solution, the estimate of **S** is incorrect. Increasing the contribution of noise to $\mathbf{S}_e$ by 30% accounted for this, resulting in values of 65 to 70%.

S was found to provide a poor indication of retrieval errors due to biases in radiance, temperature, water vapour, or cloud height. This is likely because the inverse retrieval is based on an assumption of unbiased, normally distributed errors. For biases in radiance, water vapour, and for errors in cloud height, **S** is particularly non-representative for COD, for which only 11 to 25% of cases fall within one standard deviation for **S** (for other properties the range is 36 to 78%). Biases in temperature affect **S** similarly for COD, f_{ice}, r_{liq}, and r_{ice}, (range of 48 to 66%). This underscores the importance of removing bias errors from measurements whenever possible to ensure that **S** provides the best possible representation of errors.

5.4 Cloud vertical inhomogeneity and ice habit

Errors in retrieved microphysical properties (from spectra at 0.5 cm^{-1} resolution) due to failing to capture cloud vertical inhomogeneity are shown in Table 5. For the upper set of cases shown in the table, errors were not imposed and true cloud heights were used. In performing the retrieval the correct cloud base and top were used, but the cloud was assumed to be vertically homogeneous in terms of COD and phase; thus the cloud model is accurate for dense and diffuse clouds but not for inhomogeneous or liquid-topped clouds. This emulates a measurement where the cloud base and top are known from an ancillary instrument such as a lidar. As expected, therefore, errors are similar for dense and diffuse clouds. For inhomogeneous clouds, which are thinner at the upper and lower edges, errors are slightly larger for τ_g. The largest retrieval errors are found to be for liquid-topped clouds, particularly for τ_g and f_{ice}, for which errors are about five times as large. These errors are large because the cloud heights are effectively wrong for the liquid and ice layers of the cloud. A lidar that can classify phase would allow reduction of these errors down to the level seen for other cloud types. The enhancement of errors in liquid-topped clouds relative to other cloud types disappears when errors are imposed on the observations (imposed noise of 0.2 RU, radiation bias of 0.2 RU, temperature bias of 0.2 K, and water vapour bias of -3%; see the last two sets of cases in Table 5). This is true when true cloud heights are used (middle set) and when they are retrieved (lowest set). (Similar trends are found when the radiation bias is increased to 0.5 RU, as shown in the Supplemental).

Errors in retrieved microphysical properties (from spectra at 0.5 cm^{-1} resolution) due to assuming a spherical ice habit are shown in Table 6. The first column of the table shows the true ice habit. The upper set of data has no other imposed errors, while the lower two sets have the same imposed errors as for vertically-varying clouds. Retrieval error in r_{liq} is not shown because clouds were mainly ice. In the absence of imposed errors, compared to spheres, the increase in error is greatest for τ_g, for which errors increase by an order of magnitude or more. This large increase suggests that errors in habit mainly bias the magnitude rather than spectral shape of the cloud emissivity. Overall, errors are the smallest for solid columns. However, differences in errors based on assumed ice habit diminish when errors exist in observations and cloud heights are

Penny Rowe 8/20/2019 9:42 AM
Deleted: calculated as shown in Fig. 1). Model …. The lowest model errors are ... [33]

Penny Rowe 8/20/2019 9:42 AM
Deleted: indicating…uggesting that ... [34]

Penny Rowe 8/20/2019 9:42 AM
Deleted: The… was found to provid ... [35]

Penny Rowe 8/20/2019 9:42 AM
Deleted: Ice

Penny Rowe 8/20/2019 9:42 AM
Deleted: In addition to understanding how errors affect the retrievals for the base set of idealized clouds, discussed previously, it is import to understand what effects variability in clouds will have on the retrieval. For this purpose we use the set of 92 cases used to test the effects of cloud inhomogeneity, described in Sect. 2, which are comprised of 23 cases each of dense, diffuse, inhomogeneous (thinner at the bounds) and liquid-topped clouds.
The middle set of cases shown in Table 4 includes imposed noise of 0.1 mW/(m^2 sr cm^{-1}) and temperature bias of 0.1 K, and uses retrieved cloud heights; the middle set uses true cloud heights while the final set uses retrieved cloud heights (error combinations e and f). These imposed errors are the same as those used to retrieve cloud height in Rowe et al (2016; see Table 3). When the error is imposed, retrieval error increases only slightly for this level of imposed errors.
... [36]

Penny Rowe 8/20/2019 9:42 AM
Deleted: The middle set of cases shown in includes imposed noise of 0.1 mW/(m^2 sr cm^{-1}) and temperature bias of 0.1 K, and uses retrieved cloud heights; the middle set uses true cloud heights while the final set uses retrieved cloud heights (error combinations e and f). These imposed errors are the same as those used to retrieve cloud height in Rowe et al (2016; see Table 3). When the error is imposed, retrieval error increases only slightly for this level of imposed errors.
... [37]

retrieved (bottom set). Thus, using a realistic ice habit can minimize errors, but this becomes less important when cloud height is also retrieved.

6 Conclusions

This work explores the capability of a low-resolution IR spectrometer for retrieving cloud properties in polar regions. To this end, the CLoud and Atmospheric Radiation Retrieval Algorithm (CLARRA) was used to retrieve cloud effective height (Rowe et al 2016) and microphysical properties (COD, ice fraction, effective radius of liquid, and effective radius of ice) from simulations of surface-based IR downwelling radiances, to determine the effect of instrument resolution on accuracy. CLARRA includes a method for calculating gaseous transmission and emission terms at the effective instrument resolution, minimizing model errors. A fast forward retrieval rapidly retrieves preliminary cloud microphysical properties, which then serve as inputs into an optimal nonlinear inverse method. Cloud properties were retrieved from 222 simulated radiances based on atmospheric and cloud conditions characteristic of the Arctic, with additional tests of sensitivity to cloud vertical inhomogeneity and ice habit.

Sensitivity studies for vertically-varying clouds indicate that, in the absence of observational errors, errors in retrieved microphysical properties are highest for liquid-topped clouds that are assumed to be homogeneously mixed-phase (relative to clouds that are dense, diffuse, or inhomogeneous vertically). However, in the presence of errors in observations, the gap in retrieved microphysical property errors between liquid-topped clouds and other cloud structures disappears. Future work is needed to assess errors when multiple clouds are present. For different ice habits, sensitivity studies indicate that use of a reasonable guess for the ice habit can help minimize errors, but these differences become minor in the presence of observational errors.

Retrieval accuracy was determined as a function of resolution for model errors, CHR errors, and a variety of imposed observational errors, including random noise as well as biases in the measured spectrum and atmospheric state. In the absence of imposed errors, errors in retrieved microphysical properties were found to be 0.007 for COD, 0.03 for f_{ice}, 0.7 for µm r_{liq}, and 3 µm for r_{ice} (0.5 cm^{-1} resolution; COD between 0.4 and 5). In the presence of imposed errors, errors in retrieved COD and ice fraction were found to be strongly affected by bias errors in cloud height, which in turn are high when the CHR is used. Furthermore, CHR errors typically decrease with decreasing cloud base height (Rowe et al 2016), with consequences for microphysical property retrievals. For example, for a combination of errors including noise of 0.2 RU, radiation bias of 0.2 RU, temperature bias of 2 K, water vapour bias of -3%, and CHR errors (at 4.0 cm^{-1} resolution), comparing clouds with bases above 2 km to those with bases below, the rms error decreases from 1.1 to 0.15 for COD and from 0.3 to 0.18 for f_{ice}, pointing to a strong potential for retrievals of low clouds.

Retrieval errors were found to be fairly invariant to resolution up to about 4 cm^{-1}, after which accuracy declined. For example, at 0.5 cm^{-1} resolution, for the combination of errors given above, rms retrieval errors (for clouds at all heights) are 0.7 for COD, 0.2 for f_{ice}, 3 µm for r_{liq}, and 8 µm for r_{ice}. At 4 cm^{-1} these errors are similar (0.6, 0.2, 2, and 8, respectively). Taken together, this lack of sensitivity to resolution indicates that a moderately low resolution (~ 4 cm^{-1}) surface-based IR spectrometer could provide cloud property retrievals with accuracy comparable to existing higher resolution instruments. Furthermore, these retrievals would be particularly useful for low-level clouds, for which accuracy is likely to be highest.

Penny Rowe 8/20/2019 9:42 AM
Deleted:

Penny Rowe 8/20/2019 9:42 AM
Deleted: introduces

Penny Rowe 8/20/2019 9:42 AM
Deleted:), which retrieves

Penny Rowe 8/20/2019 9:42 AM
Deleted: surface-based infrared downwelling radiance measurements made in Polar Regions. Cloud height retrievals use the CO_2 slicing method (Rowe et al 2016 and references therein). CLARRA rapidly retrieves first-guess cloud microphysical properties from a fast forward model that ignores scattering, and then uses the first-guess values as inputs into an optimal nonlinear inverse method using the Levenberg-Marquadt algorithm. Comparison of the diagonals of the covariance matrix resulting from the inverse retrieval to actual retrieval errors suggested that the covariance matrix slightly underestimates errors at the 68% confidence interval; this is correctable by increasing model errors (~0.02 RU) and estimated measurement error due to noise (by ~25%). However, it should be noted that retrieval errors are still underestimated by the covariance matrix at higher confidence ... [38]

Penny Rowe 8/20/2019 9:42 AM
Deleted: in order to improve computational efficiency. Forward model errors were ... [39]

Penny Rowe 8/20/2019 11:01 AM
Formatted: Right: 0.26"

Penny Rowe 8/20/2019 9:42 AM
Deleted: Comparison of the diagonals of covariance matrix resulting from the in ... [40]

Penny Rowe 8/20/2019 9:42 AM
Deleted: ; furthermore, errors are only slightly higher when cloud heights are ... [41]

Penny Rowe 8/20/2019 9:42 AM
Deleted: using known cloud base and top. Errors in retrieved microphysical prop ... [42]

Penny Rowe 8/20/2019 9:42 AM
Deleted: vertically

Penny Rowe 8/20/2019 9:42 AM
Deleted: clouds (having thinner upper and lower boundaries), regardless of error.

Penny Rowe 8/20/2019 9:42 AM
Deleted: error magnitudes

Penny Rowe 8/20/2019 9:42 AM
Deleted: becomes smaller as imposed errors grow

Penny Rowe 8/20/2019 9:42 AM
Deleted: .

Penny Rowe 8/20/2019 10:18 AM
Deleted:

Penny Rowe 8/20/2019 10:18 AM
Deleted: ... [43]

7 Code and data availability

Simulated radiances at monochromatic resolution (Cox et al 2015) are available by email to the corresponding author. Computer code is available at Bitbucket (https://bitbucket.org/%7B4e9c3a2c-5ac5-40f9-a7e4-0c9578f88b21%7D/), including repositories containing Python computer code (runDisort_py; https://bitbucket.org/clarragroup/rundisort_py/src/master/) and Matlab/Octave computer code (runDisort_mat; https://bitbucket.org/clarragroup/rundisort_mat/src/master/) for creating cloudy-sky spectra using DISORT (Stamnes et al 1988). See also Rowe et al (2013; 2016).

8 Author contribution

Steven Neshyba calculated Legendre moments and single-scatter albedo from single-scattering parameters. Christopher Cox led creation of simulated spectra used in this work. Von Walden conceived of the idea and provided guidance. Penny Rowe performed all other calculations and wrote the manuscript with input from all authors.

Appendix

A.1 Approximations for cloud-height retrievals

To solve the radiative transfer equation in LBLRTM and DISORT (Stamnes et al 1988), the atmosphere is divided into model atmospheric layers and the approximation is made that the Planck function varies linearly with optical depth through the layer (Wiscomb et al 1976, Clough et al 1992). In the absence of scattering, the downwelling radiance from a layer at a given wavenumber is approximated as

$$\Delta\tilde{R}_L = \int_{\tilde{\tau}_{L-1}}^{\tilde{\tau}_L} \tilde{B}(\tilde{\tau}) e^{-\tilde{\tau}\sec\theta} d\tilde{\tau} \qquad \text{(A1)}$$

where the tildes indicate monochromatic, or perfect, resolution (all quantities with tildes depend on wavenumber), τ is defined as the vertical optical depth from the surface up to some height (e.g. within layer L), τ_{L-1} is from the surface to the layer bottom, and τ_L is from the surface to the layer top. (Parentheses are used here and below to indicate dependence.) $\tilde{B}$ is the Planck function and θ is the viewing angle from zenith. Note that the formulation here differs from that of Clough et al (1992); here, R_L, τ_L, and the transmittance, t_L (defined below) are defined from the bottom of the model atmosphere (e.g. from Earth's surface), to the top of layer L. Quantities that are for layer bottom to top only are indicated with a delta. Using these conventions means that Eq. (1) represents the radiance from layer L that is transmitted by the atmosphere below to the surface. The viewing angle is included explicitly here so that τ refers to the vertical optical depth.

The surface-to-layer top transmittance depends on the the optical depth,

$$\tilde{t}_L = \exp(-\tilde{\tau}_L \sec\theta). \qquad \text{(A2)}$$

The linear-in-optical depth approximation for B allows the integral to be solved, yielding

Penny Rowe 8/20/2019 9:42 AM
Deleted: on the Arctic Observing Network (AON) Arctic data repository (https://arcticdata.io/catalog/#view/doi:10.5065/D61J97TT); updated versions with errors corrected are available

Penny Rowe 8/20/2019 9:42 AM
Deleted: ,

Penny Rowe 8/20/2019 9:42 AM
Moved (insertion) [3]

Penny Rowe 8/20/2019 11:02 AM
Formatted: Tabs: 6.67", Left

Penny Rowe 8/20/2019 9:42 AM
Moved (insertion) [4]

Penny Rowe 8/20/2019 9:42 AM
Moved (insertion) [5]

Penny Rowe 8/20/2019 9:42 AM
Moved (insertion) [6]

Penny Rowe 8/20/2019 9:42 AM
Moved (insertion) [7]

Penny Rowe 8/20/2019 9:42 AM
Moved (insertion) [10]

Penny Rowe 8/20/2019 11:02 AM
Formatted: Tabs: 6.67", Left

Penny Rowe 8/20/2019 9:42 AM
Moved (insertion) [8]

$$\Delta\tilde{R}_L = -\tilde{B}_L\tilde{t}_L + \tilde{B}_{L-1}\tilde{t}_{L-1} - \Delta\tilde{B}_L\left[\frac{\Delta\tilde{t}_L}{\Delta\tilde{\tau}_L}\right] \qquad \text{(A3)}$$

Penny Rowe 8/20/2019 11:02 AM
Formatted: Tabs: 6.67", Left

Penny Rowe 8/20/2019 9:42 AM
Moved (insertion) [9]

where $\tilde{B}_{L-1}$ and $\tilde{B}_L$ are the Planck functions of the temperature at the lower and upper boundary of layer L, and the deltas indicate the change across the layer. (Note that $\Delta\tilde{R}_L$ is calculated slightly differently in LBLRTM, following Clough et al. 1992; the two methods give similar results).

Thus ΔR_L is the radiance from the layer that makes it to the surface. The total (clear-sky) radiance is the sum of all the layer radiances. To match instrument resolution, the clear sky radiance needs to be convolved with the instrument lineshape S,

$$R_{clr}(\nu) = \int_{-\infty}^{\infty} \sum_L \Delta\tilde{R}_L(\tilde{\nu})\, S(\nu,\tilde{\nu})\, d\tilde{\nu}, \qquad \text{(A4)}$$

Penny Rowe 8/20/2019 11:03 AM
Formatted: Tabs: 6.67", Left

Penny Rowe 8/20/2019 9:42 AM
Moved (insertion) [11]

where the dependence on wavenumber has been included explicitly. Eqn (A4) can also be calculated directly by running LBLRTM and convolution with the S (typically a sinc function). We will use R_{clr} calculated in this manner to test the remaining approximations.

In practice the integral need only be performed over the small wavenumber region characterized by the width of S (typically a sinc function). Switching the order of the sum and the integral, we have

Penny Rowe 8/20/2019 9:42 AM
Moved (insertion) [12]

$$R_{clr}(\nu) \approx \sum_L \Delta R_L(\nu). \qquad \text{(A5)}$$

Penny Rowe 8/20/2019 9:42 AM
Moved (insertion) [20]

where

$$\Delta R_L(\nu) \equiv \int_{-\infty}^{\infty} \Delta\tilde{R}_L(\tilde{\nu}) S(\nu,\tilde{\nu})\, d\tilde{\nu}, \qquad \text{(A6)}$$

In addition to R_{clr}, the cloud-height retrieval (Rowe et al 2016) requires the gaseous radiance from the surface up to each possible cloud layer (R_c), which can also be calculated from ΔR_L,

$$R_c \approx \sum_{L=1}^{c} \Delta R_L. \qquad \text{(A7)}$$

Finally, the cloud height retrieval requires the transmittance of the atmosphere below the cloud (t_L; in Rowe et al 2016 it is referred to as t_c) at the effective instrument resolution. Examining Eqns (1)-(6) shows that it is more accurate to convolve the Planck function multiplied by the surface-to-layer transmittance. Thus we define the effective transmittance from the surface to a layer as

$$t_L(\nu) \equiv \left[\int_{-\infty}^{\infty} \tilde{B}_L(\tilde{\nu})\tilde{t}_L(\tilde{\nu}) S(\nu,\tilde{\nu})\, d\tilde{\nu}\right] / B_L(\nu). \qquad \text{(A8)}$$

To summarize how these approximations are used for the cloud height retrieval, first, gaseous layer optical depths $\Delta\tilde{\tau}_L$ are computed using LBLRTM. Next, $\Delta\tilde{\tau}_L$ is summed from the surface up to each layer to get $\tilde{\tau}_L$. Eqn (A2) is then used to calculate $\tilde{t}_L$, and Eqns (A3) and (A6) are used to calculate ΔR_L. Equation (A5) is used to calculate R_{clr}, and Eqn (A7) is used to calculate R_c for each model layer that could contain cloud (for cloud heights within layers, terms are interpolated). Equation (A8) is used to calculate t_L.

A.2 Approximations and model error for cloud microphysical property retrievals

Retrieval of microphysical cloud properties requires effective-resolution layer optical depths, $\Delta\tau_L$, as input into the DISORT radiative transfer code. One method to create the set of $\Delta\tau_L$ might be to reduce the resolution of the layer optical depths. However, the above equations suggest that a more accurate method would be in terms of transmittances. Inserting Eq. (A2) into Eq. (A6) and breaking up the integral gives

$$\Delta R_L(\nu) = -\int_{-\infty}^{\infty} \tilde{B}_L \tilde{t}_L S(\nu,\tilde{\nu})d\tilde{\nu} + \int_{-\infty}^{\infty} \tilde{B}_{L-1} \tilde{t}_{L-1} S(\nu,\tilde{\nu})d\tilde{\nu} - \int_{-\infty}^{\infty} \Delta\tilde{B}_L \left[\frac{\Delta\tilde{t}_L}{\Delta\tilde{\tau}_L}\right] S(\nu,\tilde{\nu})d\tilde{\nu}. \qquad \text{(A9)}$$

The first two terms on the right hand side of this equation have the same form as the integral in Eqn (A8) and can be replaced with $-B_L t_L$ and $B_{L-1} t_{L-1}$. Thus it makes sense to create the set of $\Delta\tau_L$ using t_L (noting that the third term in Eqn (A9) also includes the monochromatic layer gaseous optical depth and thus represents a source of error).

Due to ringing, t_L can be greater than 1 or less than 0, resulting in optical depths outside physical bounds. To minimize ringing, transmittances were averaged over small spectral regions between strong emission lines, or microwindows (Table 2). Observed radiances are therefore also averaged over microwindows. (Note that it might be more accurate to average the term in brackets in Eqn. (A8); an alternate option would be to use an apodization function rather than a sinc function in Eqn. (A8) to reduce ringing; these are both interesting topics for future work). Following this, transmittances below 10^{-40} and above 1 were modified such that $10^{-40} <= t_L <= 1$.

Finally, layer optical are calculated from t_L. For the first layer,

$$\Delta\tau_1 \equiv -\log(t_1). \qquad \text{(A10)}$$

For subsequent layers, the optical depths of all layers below must be subtracted.

$$\Delta\tau_L \equiv -\log(t_L) - \sum_{x=1}^{L-1} \Delta\tau_x. \qquad \text{(A11)}$$

The advantage of approximating radiances using layer optical depths derived from surface-to-layer transmittances convolved to the instrument resolution is shown in Fig. 4. Errors for this convolved-transmittance (CT) method are compared to errors for radiances calculated using optical depths derived from averaged monochromatic surface-to-layer transmittances (or from averaged monochromatic layer optical depths). In Fig. 4a averages are over the wavenumber spacing. Fig. 4b shows averages over microwindows, used in the cloud microphysical retrievals. (For simplicity, clouds are omitted from this example). Errors are determined by comparison with R_{clr} calculated as in Eqn. (A4), using LBLRTM and then convolving to the desired resolution (0.5 cm^{-1} here), and (in b), averaged over microwindows. Errors are reduced significantly by the CT method, relative to the other approximations. In microwindows used in the cloud microphysical property retrieval (Fig 4b), errors are within 3 or 30 RU for the other methods, whereas for the CT method they are <= 0.01

Penny Rowe 8/20/2019 9:42 AM
Moved (insertion) [13]

Penny Rowe 8/20/2019 9:42 AM
Moved (insertion) [14]

Penny Rowe 8/20/2019 9:42 AM
Moved (insertion) [15]

Penny Rowe 8/20/2019 11:01 AM
Formatted: Right: 0.26", Tabs: 6.67", Left

Penny Rowe 8/20/2019 10:59 AM
Deleted:

Penny Rowe 8/20/2019 9:42 AM
Moved (insertion) [18]

Penny Rowe 8/20/2019 9:42 AM
Moved (insertion) [19]

Penny Rowe 8/20/2019 9:42 AM
Moved (insertion) [16]

Penny Rowe 8/20/2019 9:42 AM
Moved (insertion) [21]

Penny Rowe 8/20/2019 9:42 AM
Moved (insertion) [17]

(for this clear-sky example; the range for cloudy cases used in this work is shown in Fig. 1); thus the CT method represents a significant improvement. Finally, it is worth noting that errors at instrument resolution are also fairly low (Fig. 4a). This is shown here for reference only, and is not used in this work, but has the potential for use in a cloud-property retrieval that includes scattering, using DISORT.

To summarize the approximations used for the cloud microphysical property retrievals, the set of effective-resolution gaseous layer optical depths needed for running DISORT are calculated as follows. The first few steps are the same as for the cloud height retrieval: $\Delta\tilde{\tau}_L$ is computed using LBLRTM and these are summed from the surface to each layer to get $\tilde{\tau}_L$, and Eqn (A2) is used to calculate $\tilde{t}_c$. Next, Eqn (A8) is used to calculate t_c, which is then averaged over microwindows and bounded to be between 10^{-40} and 1. Eqns (A10) and (A11) are then used to calculate $\Delta\tau_L$. Since DISORT is run at single precision, serious errors can result for very small input optical depths, thus $\Delta\tau_L$ was increased as needed such that $\Delta\tau_L >= 10^{-5}$.

Acknowledgements

This work was funded by National Science Foundation grants ARC-1108451 and PLR 1543236. S. N. acknowledges NSF Grant CHE 1807898. Computer code was written in the Python computing language and figures were created using Matplotlib. We are grateful for help with Python coding from Daniel Neshyba-Rowe and for advice on running DISORT from Istvan Laszlo.

References

Boucher, O., D. Randall, P. Artaxo, C. Bretherton, G. Feingold, P. Forster, V.-M. Kerminen, Y. Kondo, H. Liao, U. Lohmann, P. Rasch, S.K. Satheesh, S. Sherwood, B. Stevens and X.Y. Zhang, Clouds and Aerosols. In: Climate Change 2013: The Physical Science Basis. Contribution of Working Group I to the Fifth Assessment Report of the Intergovernmental Panel on Climate Change [Stocker, T.F., D. Qin, G.-K. Plattner, M. Tignor, S.K. Allen, J. Boschung, A. Nauels, Y. Xia, V. Bex and P.M. Midgley (eds.)]. Cambridge University Press, Cambridge, United Kingdom and New York, NY, USA, 2013.

Bromwich, D. H., Nicolas, J. P., Hines, K. M., Kay, J. E., Key, E. L., Lazzara, M. A., et al.: Tropospheric clouds in Antarctica. Reviews of Geophysics, 50, RG1004. http://doi.org/10.1029/2011RG000363, 2012.

Clough, S., Iacono, M. J., & Moncet, J. L.: Line-by-line calculations of atmospheric fluxes and cooling rates: Application to water vapour. Journal of Geophysical Research: Atmospheres, 97(D14), 15761–15785, 1992.

Clough, S., Shephard, M. W., Shephard, M. W., Mlawer, E. J., Delamere, J. S., Iacono, M. J., et al.: Atmospheric radiative transfer modeling: a summary of the AER codes. Journal of Quantitative Spectroscopy and Radiative Transfer, 91(2), 233–244. http://doi.org/10.1016/j.jqsrt.2004.05.058, 2005.

Cox, C., Turner, D. D., Rowe, P. M., Shupe, M., & Walden, V. P.: Cloud Microphysical Properties Retrieved from Downwelling Infrared Radiance Measurements Made at Eureka, Nunavut, Canada (2006–09). Journal of Applied Meteorology and Climatology, 53(3), 772–791, http://doi.org/20.1175/JAMC-D-13-0113.1, 2014

Penny Rowe 8/20/2019 9:42 AM
Deleted: vapor

Cox, C., Walden, V. P., Rowe, P. M., & Shupe, M.: Humidity trends imply increased sensitivity to clouds in a warming Arctic. Nature Communications, 6, 10117. http://doi.org/10.1038/ncomms10117, 2015.

Dee, D. P., Uppala, S. M., Simmons, A. J., Berrisford, P. , Poli, P. , Kobayashi, S. , Andrae, U. , Balmaseda, M. A., Balsamo, G. , Bauer, P. , Bechtold, P. , Beljaars, A. C., van de Berg, L. , Bidlot, J. , Bormann, N. , Delsol, C. , Dragani, R. , Fuentes, M. , Geer, A. J., Haimberger, L. , Healy, S. B., Hersbach, H. , Hólm, E. V., Isaksen, L. , Kållberg, P. , Köhler, M. , Matricardi, M. , McNally, A. P., Monge-Sanz, B. M., Morcrette, J. , Park, B. , Peubey, C. , de Rosnay, P. , Tavolato, C. , Thépaut, J. and Vitart, F.: The ERA-Interim reanalysis: configuration and performance of the data assimilation system. Q.J.R. Meteorol. Soc., 137: 553-597. doi:10.1002/qj.828, 2011.

Francis, J. A., and Hunter, E.: New insight into the disappearing Arctic sea ice, Eos Trans. AGU, 87(46), 509– 511, doi:10.1029/2006EO460001, 2006.

Garrett, T. and Zhao, C.: Ground-based remote sensing of thin clouds in the Arctic, Atmos. Meas. Tech., 6, 1227–1243, doi:10.5194/amt-6-1227, 2013.

Hines, K. M., Bromwich, D. H., Rasch, P., & Iacono, M. J.: Antarctic Clouds and Radiation within the NCAR Climate Models. Journal of Climate, 17(6), 1198–1212, 2004.

Kay, J. E., and Gettelman, A.: Cloud influence on and response to seasonal Arctic sea ice loss, J. Geophys. Res., 114, D18204, doi:10.1029/2009JD011773, 2009.

Komurcu, M., Storelvmo, T., Tan, I., Lohmann, U., Yun, Y., Penner, J.E., Wang, Y., Liu, X., and Takemura, T.: Intercomparison of the cloud water phase among global climate models, J. Geophys. Res. Atmos.,119, 3372– 3400, doi:10.1002/2013JD021119, 2014.

Lachlan-Cope, T., Listowski, C., and O'Shea, S.: The microphysics of clouds over the Antarctic Peninsula – Part 1: Observations. Atmospheric Chemistry and Physics, 16 (24). 15605-15617, doi:10.5194/acp-16-15605, 2016.

Lawson, R.P, and Gettelman, A.: Impact of Antarctic clouds on climate, PNAS 111 (51) 18156-18161, doi:10.1073/pnas.1418197111, 2014.

L'Ecuyer T.S., Jiang J.H.: Touring the atmosphere aboard the A-Train. Phys Today 63(10):36–4, doi:10.1063/1.3463626, 2010.

L'Ecuyer, T.S., Y. Hang, A.V. Matus, and Z. Wang, Z: Reassessing the effect of cloud type on Earth's energy balance in the age of active spaceborne observations. Part I: Top-of-atmosphere and surface. *J. Climate,* 0, https://doi.org/10.1175/JCLI-D-18-0753.1, 2019.

Mahesh, A., Walden, V. P., & Warren, S. G.: Ground-based infrared remote sensing of cloud properties over the Antarctic Plateau. Part II: Cloud optical depths and particle sizes. Journal of Applied Meteorology, 40(7), 1279–1294, 2001.

Palchetti, L., Bianchini, G., Di Natale, G., and Del Guasta, M.: Far-Infrared Radiative Properties of Water Vapour and Clouds in Antarctica. Bull. Amer. Meteor. Soc., 96, 1505–1518, doi:10.1175/BAMS-D-13-00286.1, 2015.

Poulsen et al., 2012: Retrievals from satellite data using optimal estimation: evaluation and application to ATSR, Atmos. Meas. Tech., 5, 1889-1910.

Penny Rowe 8/20/2019 9:42 AM

Deleted: L'Ecuyer, T.S., P. Gabriel, K. Leesman, S.J. Cooper, and G.L. Stephens, 2006: Objective Assessment of the Information Content of Visible and Infrared Radiance Measurements for Cloud Microphysical Property Retrievals over the Global Oceans. Part I: Liquid Clouds. *J. Appl. Meteor. Climatol.*, 45, 20–41, doi: 10.1175/JAM2326.1

Penny Rowe 8/20/2019 9:42 AM

Deleted: Vapor

Peters, W., Jacobson, A. R., Sweeney, C. , Andrews, A. E. , Conway, T. J., Masarie, K., Miller, J. B., Bruhwiler, L. M. P., Petron, G., Hirsch, A. I. , D. E. J. Worthy, G. R. van der Werf, J. T. Randerson, P. O. Wennberg, M. C. Krol, and P. P. Tans. An atmospheric perspective on North American carbon dioxide exchange: CarbonTracker. PNAS, 104:18925–18930, doi:10.1073/pnas.0708986104, 2007.

Rathke, C. & Fischer, J.: Retrieval of Cloud Microphysical Properties from Thermal Infrared Observations by a Fast Iterative Radiance Fitting Method. *J. Atmos. Oceanic Technol.*, 17, 1509–1524, 2000.

Rathke, C., Fischer, J., Neshyba, S., & Shupe, M.: Improving IR cloud phase determination with 20 microns spectral observations. Geophysical Research Letters, 29(8), 50–1–50–4, doi:10.1029/2001GL014594, 2002a.

Rathke, C., Neshyba, S., Shupe, M., Rowe, P., & Rivers, A.: Radiative and microphysical properties of Arctic stratus clouds from multiangle downwelling infrared radiances. Journal of Geophysical Research, 107(D23), AAC 12–1–AAC 12–13, 2002b.

Rowe, P. M., Miloshevich, L. M., Turner, D. D., & Walden, V. P.: Dry Bias in Vaisala RS90 Radiosonde Humidity Profiles over Antarctica. Journal of Atmospheric and Oceanic Technology, 25(9), 1529–1541. http://doi.org/10.1175/2008JTECHA1009.1, 2008.

Rowe, P. M., Neshyba, S., & Walden, V. P.: Radiative consequences of low-temperature infrared refractive indices for supercooled water clouds. Atmospheric Chemistry and Physics, 13(23), 11925–11933, 2013.

Rowe, P. M., Cox, C., & Walden, V. P.: Toward autonomous surface-based infrared remote sensing of polar clouds: Cloud height retrievals. Atmospheric Measurement Techniques, 9, 3641–3659, doi:10.5194/amt-9-3641, 2016.

Silber, I., Verlinde, J., Eloranta, E. W., & Cadeddu, M.: Antarctic cloud macrophysical, thermodynamic phase, and atmospheric inversion coupling properties at McMurdo Station: I. Principal data processing and climatology. Journal of Geophysical Research: Atmospheres, 123, 6099– 6121, doi:10.1029/2018JD028279, 2018.

Stamnes, K., Tsay, S.-C., Wiscombe, W. J., and Jayaweera, K.: Numerically stable algorithm for discrete-ordinate-method radiative transfer in multiple scattering and emitting layered media, Appl. Optics, 27, 2502–2509, doi:10.1364/AO.27.002502, 1988.

Turner, D. D.: Arctic mixed-phase cloud properties from AERI lidar observations: Algorithm and results from SHEBA. Journal of Applied Meteorology, 44(4), 427–444, 2005.

Uttal, T., Starkweather, S., Drummond, J. R., Vihma, T., Makshtas, A. P., Darby, L. S., et al.: International Arctic Systems for Observing the Atmosphere (IASOA): An International Polar Year Legacy Consortium. Bulletin of the American Meteorological Society, BAMS–D–14–00145.1, doi:10.1175/BAMS-D-14-00145.1, 2015.

van den Broeke, M., Box, J., Fettweis, X., Hanna, E., Noël, B., Tedesco, M., et al. (2017): Greenland Ice Sheet Surface Mass Loss: Recent Developments in Observation and Modeling. Current Climate Change Reports, 3(4), 345–356, doi:10.1007/s40641-017-0084-8, 2017.

Wagner, R., Benz, S., Möhler, O., Saathoff, H., Schnaiter, M., & Schurath, U.: Mid-infrared Extinction Spectra and Optical Constants of Supercooled Water Droplets. The Journal of Physical Chemistry A, 109(32), 7099–7112, doi:10.1021/jp051942z, 2005.

Walden, V. P., Town, M. S., Halter, B., & Storey, J.: First measurements of the infrared sky brightness at Dome C, Antarctica. Publications of the Astronomical Society of the Pacific, 117(829), 300–308, doi:10.1086/427988, 2005.

Wang, Y., Yuan, X., Bi, H., Liang, Y., Huang, H., Zhang, Z., & Liu, Y.: The contributions of winter cloud anomalies in 2011 to the summer sea-ice rebound in 2012 in the Antarctic. Journal of Geophysical Research: Atmospheres, 124, 3435–3447. https://doi.org/10.1029/2018JD029435, 2019.

Wang, X. and Key, J.R.: Arctic Surface, Cloud, and Radiation Properties Based on the AVHRR Polar Pathfinder Dataset. Part II: Recent Trends. J. Climate, 18, 2575–2593, doi:10.1175/JCLI3439.1, 2005.

Wang, C., S. Platnick, Z. Zhang, K. Meyer, and P. Yang, 2016: Retrieval of ice cloud properties using an optimal estimation algorithm and MODIS infrared observations: 1. Forward model, error analysis, and information content, *J. Geophys. Res. Atmos.*, **121**, 5809–5826, doi:10.1002/ 2015JD024526.

Warren, S. G., & Brandt, R. E.: Optical constants of ice from the ultraviolet to the microwave: A revised compilation. Journal of Geophysical Research, 113(D14), D14220, doi: 10.1029/2007JD009744, 2008.

Wesslen, C., Tjernstrom, M., Bromwich, D.H., de Boer, G., Ekman, A. M. L., Bai, L.-S., and Wang, S.-H.: The Arctic summer atmosphere: an evaluation of reanalysis using ASCOS data. Atmos. Chem. Phys. 14, 2605-2624, doi:10.5194/acp-14-2605-214, 2014.

Wiscombe, W. J.: Extension of the doubling method to inhomogeneous sources. JQSRT, 16(6), 477–489, 1976.

Winker, D., Chepfer, H., Noel, V. and Cai, X.: Observational Constraints on Cloud Feedbacks: The Role of Active Satellite Sensors, Surv. Geophys. 38: 1483, doi:10.1007/s10712-017-9452-0, 2017.

Yang, P., Bi, L., Baum, B. A., Liou, K. N., Kattawar, G. W., Mishchenko, M. I., and Cole, B.: Spectrally Consistent Scattering, Absorption, and Polarization Properties of Atmospheric Ice Crystals at Wavelengths from 0.2 to 100 µm, J. Atmos. Sci., 70, 330–347, doi:10.1175/JAS-D-12-039.1, 2013.

Zasetsky, A. Y., Khalizov, A. F., Earle, M. E., Sloan, J. J., & Sloan, J. J.: Frequency Dependent Complex Refractive Indices of Supercooled Liquid Water and Ice Determined from Aerosol Extinction Spectra. The Journal of Physical Chemistry A, 109(12), 2760–2764. doi:/10.1021/jp044823c, 2005.

Table 1. Statistics of cloud microphysical properties. Standard deviations were calculated for the logarithms of cloud optical depth referenced to the geometric limit (τ_g), effective radius of liquid (r_{liq}) and effective radius of ice (r_{ice}) because distributions for the logarithms were found to be more Gaussian in shape; these standard deviations were converted positive and negative standard deviations for these quantities. The ice fraction, f_{ice}, peaks strongly at both limits; thus no standard deviation is provided.

Quantity	Units	Mean	Std. dev.	range
τ_g	(tau)	2	-0.5, +2	0.03 – 9.3
f_{ice}	(fract)	0.5	-	0 - 1
r_{liq}	(µm)	10	-3, +4	2 - 21
r_{ice}	(µm)	25	-9, +14	5 - 58

Penny Rowe 8/20/2019 10:04 AM
Formatted Table

Penny Rowe 8/20/2019 10:04 AM
Deleted: Quantity ... [44]

Penny Rowe 8/20/2019 9:42 AM
Deleted:

Table 2. Microwindows used in the microphysical cloud property retrievals. The first column gives the central wavenumber, the second column gives the microwindow width for resoluitons of 0.1 to 4 cm^{-1}. For resolutions of 8 cm^{-1}, some microwindows were widened slightly so that there was at least one point in the microwindow (a few were narrowed so that there was only one point). Two sets of microwindows were used in this work: a combination of those used by Rathke et al (2000) and Mahesh et al (2001), indicated with superscripts R and M; and microwindows similar to those used by Turner (2005), consisting of all wavenumbers in plain font (e.g. not bold).

ν (cm^{-1})	0.1 – 4 cm^{-1} width (cm^{-1})
497.0	4.1
522.5^R	4.0
531.8^R	3.7
560.0^R	4.0
572.5^R	3.0
772.8	3.9
788.1	4.0
811.5	4.0
820.2	6.5
831.6^M	6.0
845.6	5.0
862.0^M	3.9
875.0	5.0
893.8	3.9
901.5^M	6.6
917.5^M	4.0
934.6^M	10.1
961.1^M	6.3
988.2^M	6.6
1080.7	8.2
1095.2	5.7
1115.1	3.0
1128.5	8.2
1145.1	5.8
1159.3	8.2

Table 3. Root-mean-square errors in retrieved cloud microphysical properties for base set of spectra due to model error only (no errors imposed), for spectral resolutions indicated. Errors are shown for cloud geometric optical depth (τ_g), ice fraction (f_{ice}) effective radius of liquid (r_{liq}), and effective radius of ice (r_{ice}), for four ranges in τ_g.

		0.1 cm^{-1}	0.5 cm^{-1}	4 cm^{-1}
τ_g	$\tau_g < 0.25$	0.005	0.004	0.005
	$0.25 < \tau_g < 0.4$	0.005	0.006	0.006
	$0.4 < \tau_g < 5$	0.013	0.007	0.013
	$\tau_g > 5$	0.3	0.3	0.4
f_{ice}	$\tau_g < 0.25$	0.11	0.11	0.13
	$0.25 < \tau_g < 0.4$	0.10	0.08	0.09
	$0.4 < \tau_g < 5$	0.03	0.03	0.03
	$\tau_g > 5$	0.017	0.013	0.10
r_{liq}	$\tau_g < 0.25$	4	3	4
(μm)	$0.25 < \tau_g < 0.4$	2	2	3
	$0.4 < \tau_g < 5$	0.6	0.7	0.6
	$\tau_g > 5$	0.7	0.7	1.2
r_{ice}	$\tau_g < 0.25$	7	6	8
(μm)	$0.25 < \tau_g < 0.4$	7	7	6
	$0.4 < \tau_g < 5$	4	3	3
	$\tau_g > 5$	3	3	8

Table 4. Errors in retrieved cloud microphysical properties (mean error and standard deviation of error; SD; COD refers to cloud optical depth in the geometric limit, r_{liq} and r_{ice} are the effective radii of liquid and ice) for various errors imposed on the observations (see text).

	COD		Ice fraction		r_{liq} (µm)		r_{ice} (µm)	
	Mean	SD	Mean	SD	Mean	SD	Mean	SD
None	0.001	0.007	0.00	0.03	0.0	0.9	1	3
Noise (0.2 RU)	0.00	0.03	0.00	0.13	0	1.8	0	6
Bias (0.2 RU)	-0.03	0.03	0.04	0.14	-1	1.5	-2	5
Bias (-0.2 RU)	0.03	0.03	-0.04	0.14	0	1.6	2	5
Bias (1.0 RU)	-0.12	0.13	0.04	0.17	-1	2	-5	6
Bias (-1.0 RU)	0.17	0.2	-0.08	-0.2	1	2	6	7
Temp. (0.2 K)	0.03	0.03	-0.04	0.11	0.2	1.2	2	4
Temp. (-0.2 K)	-0.01	0.09	0.00	0.19	-0.2	1.1	0	5
Temp (1.0 K)	0.15	0.2	-0.09	0.18	0	2	3	6
Temp (-1.0 K)	-0.10	0.13	0.04	0.21	0	2	-2	6
WV (3%)	0.01	0.02	-0.02	0.09	-0.3	1.5	1	5
WV (-3%)	-0.01	0.02	0.05	0.11	-0.4	1.6	-1	6
WV (10%)	0.04	0.05	-0.02	0.14	-1	2	1	6
WV (-10%)	-0.04	0.06	0.07	0.15	0	2	-2	7
CO2 Slicing	0.1	0.3	-0.04	0.14	0.3	1.4	1	4
Combined, a	-0.01	0.04	0.04	0.14	0	2	-3	7
Combined, b	0.08	0.08	-0.10	0.18	0	3	4	6
Combined, c	-0.1	0.7	0.03	0.25	0	2	-3	7
Combined, d	0.1	0.3	-0.12	0.20	1	2	4	7

Penny Rowe 8/20/2019 9:42 AM
Deleted: 3

Penny Rowe 8/20/2019 9:42 AM
Deleted: where COD refers to cloud optical depth in the geometric limit, r_{liq}

Penny Rowe 8/20/2019 9:42 AM
Deleted: r_{ice} are the effective radii of liquid and ice, and SD indicates

Penny Rowe 8/20/2019 9:42 AM
Deleted:) for base set spectra at a resolution of 0.5 cm^{-1} and optical depth between 0.4 and 5, with imposed errors on measurement and atmospheric state. Combined errors are described in the text. For PWV biases of 10% and -10% and set d of combined errors, 12, 9, and 2 points (respectively) were omitted due to having anomalously large errors. ... [45]

Penny Rowe 8/20/2019 9:42 AM
Deleted: , and SD indicates standard deviation).

Table 5. Root-mean-square errors in retrieved cloud microphysical properties for macroscopically varying clouds: cloud optical depth (COD), ice fraction (f_{ice}), and effective radii of liquid and ice (r_{liq} and r_{ice}). For the upper set of cases, errors were not imposed on observations (error = n) and true cloud heights were used. The middle set of cases includes imposed errors with true cloud heights (error = y), while the lowest set includes imposed errors with retrieved cloud heights (error = y*; see text).

Cloud type	Error	COD	f_{ice}	r_{liq} (μm)	r_{ice} (μm)
Dense	n	0.012	0.01	0.5	6
Diffuse	n	0.012	0.02	0.5	6
Inhomogeneous	n	0.019	0.02	0.5	7
Liquid topped	n	0.09	0.10	1.1	10
Dense	y	0.04	0.16	2	9
Diffuse	y	0.05	0.15	3	9
Inhomogeneous	y	0.05	0.12	2	8
Liquid topped	y	0.08	0.14	3	8
Dense	y*	0.10	0.17	2	10
Diffuse	y*	0.09	0.17	2	9
Inhomogeneous	y*	0.18	0.19	2	9
Liquid topped	y*	0.12	0.15	3	8

Table 6. Root-mean-square errors in retrieved cloud microphysical properties, assuming a spherical ice habit, for ice clouds of varying habit (first column): cloud optical depth (COD), ice fraction (f_{ice}), and effective radius of ice (r_{ice}). For the upper set of cases, errors were not imposed (error = n) and true cloud heights were used. The middle set of cases includes imposed error with true cloud heights (error = y), while the lowest set includes imposed errors with retrieved cloud heights (error = y*; see text).

Habit	Error	COD	f_{ice}	r_{ice} (µm)
Sphere	n	0.02	0.01	4
Hollow bullet rosette	n	0.6	0.07	10
Smooth solid column	n	0.3	0.03	7
Rough solid column	n	0.3	0.04	7
Smooth plate	n	0.6	0.05	7
Rough plate	n	0.5	0.07	7
Sphere	y	0.06	0.12	8
Hollow bullet rosette	y	0.6	0.09	8
Smooth solid column	y	0.3	0.07	7
Rough solid column	y	0.3	0.09	7
Smooth plate	y	0.5	0.11	9
Rough plate	y	0.5	0.10	6
Sphere	y*	0.7	0.11	6
Hollow bullet rosette	y*	0.8	0.22	8
Smooth solid column	y*	0.7	0.19	4
Rough solid column	y*	0.8	0.17	5
Smooth plate	y*	0.7	0.21	5
Rough plate	y*	0.7	0.21	4

Penny Rowe 8/20/2019 9:42 AM
Deleted: noise of 0.1 mW/(m^2 sr cm^{-1}) and temperature bias of 0.1 K,

Penny Rowe 8/20/2019 9:42 AM
Deleted:); for

Penny Rowe 8/20/2019 9:42 AM
Deleted: ,

Penny Rowe 8/20/2019 9:42 AM
Deleted: are identical except that

Penny Rowe 8/20/2019 9:42 AM
Deleted: were used

Penny Rowe 8/20/2019 9:42 AM
Deleted: *).

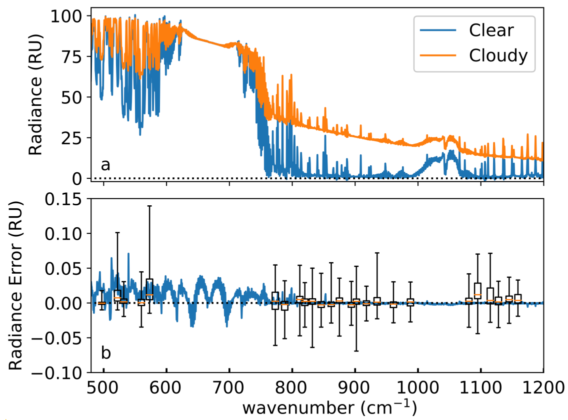

Figure 1. (a) Clear and cloudy-sky downwelling radiance (1 RU = 1 mW / [m^2 sr cm^{-1}]) for a typical polar atmosphere at a resolution of 0.5 cm^{-1} (b) Model errors (model – true) in downwelling radiances for the clear-sky radiance shown in the top panel (blue solid line), and box and whiskers plots of model errors for all radiances, averaged in microwindows (horizontal lines give the median, boxes give the 1st and 3rd quartiles, and whiskers give the range).

Unknown
Formatted: Font:10 pt

Penny Rowe 8/20/2019 9:42 AM
Deleted: cloud

Penny Rowe 8/20/2019 9:42 AM
Deleted: (top).

Penny Rowe 8/20/2019 9:42 AM
Deleted: ,

Penny Rowe 8/20/2019 9:42 AM
Deleted: ; bottom

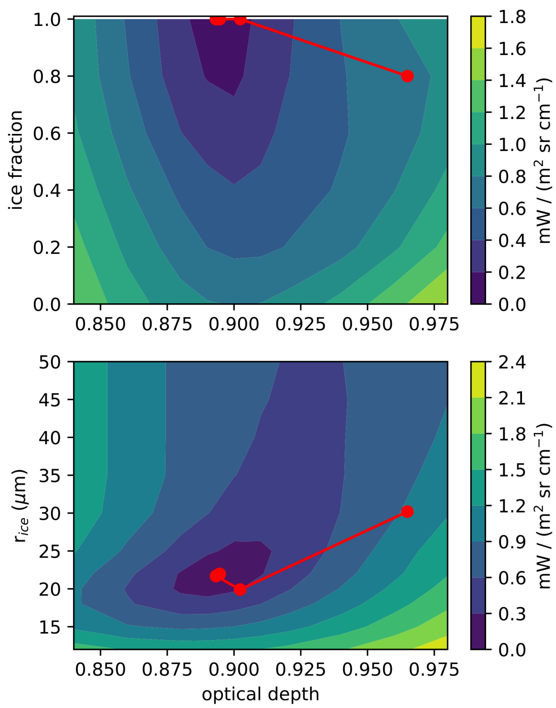

Figure 2. Error contours for retrievals of ice effective radius (r_{ice}), ice fraction, and cloud optical depth, as root-mean-square error in radiances for an ice-only cloud. The retrieval trajectory (red line) and results for each iteration (red dots) are superimposed on the contour surface.

Penny Rowe 8/20/2019 9:42 AM
Deleted: rms

Penny Rowe 8/20/2019 9:42 AM
Deleted: circles) is

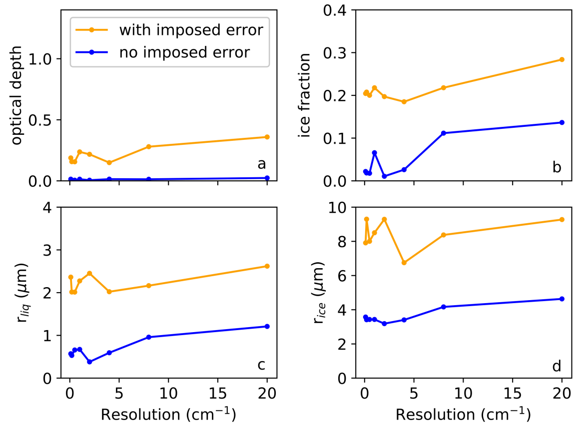

Figure 3. Root-mean-square error in retrieved microphysical cloud properties as a function of resolution, where r_{liq} is the effective radius of liquid and r_{ice} is the effective radius of ice, for cases with and without imposed error, as described in the text.

Penny Rowe 8/20/2019 9:42 AM
Deleted: Errors

Penny Rowe 8/20/2019 9:42 AM
Deleted: (mean and standard deviation; SD)

Penny Rowe 8/20/2019 9:42 AM
Deleted: no

Penny Rowe 8/20/2019 9:42 AM
Deleted: (no error) and with imposed errors

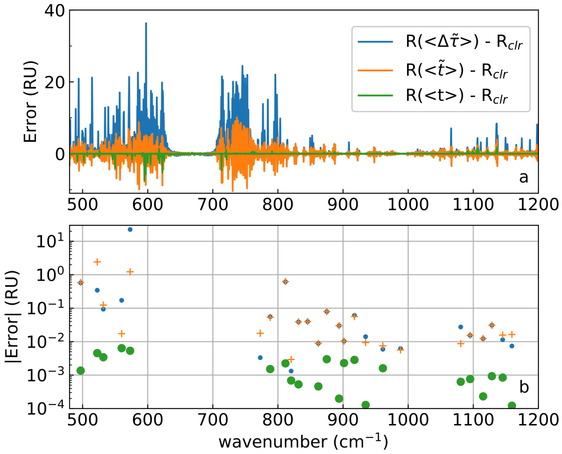

Figure 4. Radiance errors (1 RU = 1 $mW/[m^2\ sr\ cm^{-1}]$) for different methods of approximating the radiance at a resolution of 0.5 cm^{-1}. Approximate radiances are computed using averages of perfect-resolution layer optical depths $R(<\Delta\tilde{\tau}>)$, mean surface-to-layer perfect-resolution transmittances $R(<\tilde{t}>)$, or mean surface-to-layer transmittances after convolution to the instrument $R(<t>)$; averages are over 0.5 cm^{-1} (a) or over microwindows (b). Approximate radiances are compared to simulated radiances at 0.5 cm^{-1} resolution (R_{clr}), which are averaged over microwindows in (b).